Hot climate inhibits volcanism on Venus: Constraints from rock deformation experiments and argon isotope geochemistry

Sami Mikhail[1,2*] and Michael J. Heap[3]

[1]*The School of Earth and Environmental Sciences, The University of St Andrews, U.K.*

[2]*St Andrews Centre for Exoplanet Science, The University of St. Andrews, U.K.*

[3]*Géophysique Expérimentale, Institut de Physique de Globe de Strasbourg, France.*

*Corresponding author: S. Mikhail (sm342@st-andrews.ac.uk)

Abstract

The disparate evolution of sibling planets Earth and Venus has left them markedly different. Venus' hot (460 °C) surface is dry and has a hypsometry with a very low standard deviation, whereas Earth's average temperature is 4 °C and the surface is wet and has a pronounced bimodal hypsometry. Counterintuitively, despite the hot Venusian climate, the rate of intraplate volcano formation is an order of magnitude lower than that of Earth. Here we compile and analyse rock deformation and atmospheric argon isotope data to offer an explanation for the relative contrast in volcanic flux between Earth and Venus. By collating high-temperature, high-pressure rock deformation data for basalt, we provide a failure mechanism map to assess the depth of the brittle–ductile transition (BDT). These data suggest that the Venusian BDT likely exists between 2–12 km depth (for a range of thermal gradients), in stark contrast to the BDT for Earth, which we find to be at a depth of ~25-27 km using the same method. The implications for planetary evolution are twofold. First, downflexing and sagging will result in the sinking of high-elevation structures, due to the low flexural rigidity of the predominantly ductile Venusian crust, offering an explanation for

25 the curious coronae features on the Venusian surface. Second, magma delivery to the surface—the
26 most efficient mechanism for which is flow along fractures (dykes; i.e., brittle deformation)—will
27 be inhibited on Venus. Instead, we infer that magmas must stall and pond in the ductile Venusian
28 crust. If true, a greater proportion of magmatism on Venus should result in intrusion rather than
29 extrusion, relative to Earth. This predicted lower volcanic flux on Venus, relative to Earth, is
30 supported by atmospheric argon isotope data: we argue here that the anomalously unradiogenic
31 present-day atmospheric $^{40}Ar/^{36}Ar$ ratio for Venus (compared with Earth) must reflect major
32 differences in ^{40}Ar degassing, primarily driven by volcanism. Indeed, these argon data suggest that
33 the volcanic flux on Venus has been three times lower than that on Earth over its 4.56 billion year
34 history. We conclude that Venus' hot climate inhibits volcanism.
35

1 Introduction

The present-day differences in the expression and intensity of volcanism on the telluric planets serves as a testament to the dynamic nature of planetary evolution (Wilson, 2009). For example, Earth and Venus are colloquially referred to as sibling planets because of their similar mass and bulk composition (i.e., bulk petrology). However, their contrasting atmospheric mass and chemistry (e.g., Gaillard and Scaillet, 2014; Mikhail and Sverjensky, 2014), climate (e.g., Pollack et al., 1980), and geomorphology (e.g., Head and Solomon, 1981; Donahue and Russell, 1997; Basilevsky and Head, 2003; Ghail, 2015) and volcanic character (e.g., Fegley and Prinn, 1989; Head et al., 1992; Wilson, 2009) is striking: Earth is a crucible of life, whereas Venus is a barren wasteland. Suffice to say, then, Earth and Venus are not identical siblings. The major differences between Venus and Earth are discussed in detail below.

First, the average surface temperatures are 460 and 4 °C on Venus and Earth, respectively. The Earth also has an excess in surface water of about 1.2×10^{21} kg compared to Venus, a difference between five and six orders of magnitude (Donahue, 1999; Lécuyer et al., 2000). The high temperature and low water content of the Venusian surface are a combined consequence of the absence of a magnetic field (Donahue and Russell, 1997), the presence of a dense atmosphere dominated by CO_2 (at a pressure of 9 MPa), and its proximity to the Sun (with a solar irradiance of 2611 W/m^2, compared with 1366 W/m^2 on Earth).

Second, hypsometric data show that >80% of the surface elevation of Venus ranges from –1.0 to +2.5 km; only ~2% of the surface lies >2 km above the median radius (Fig. 1) (Head and Solomon, 1981; Basilevsky and Head, 2003; Taylor and McLennan, 2009). The surface of Earth, by contrast, has a pronounced bimodal hypsometry (i.e., it has continental rises and ocean basins; Fig. 1). The fact that Venus has a hypsometry with a very low standard deviation is not easily attributable to the absence of plate tectonics on Venus, because Mars—a planet that, like Venus, operates a stagnant-lid tectonic regime (Head and Solomon, 1981; Head et al., 1992; Donahue and Russell, 1997; Basilevsky and Head, 2003)—has a surface hypsometry with a very large standard deviation (Fig.

62 1).

63 Third, the way in which volcanism is manifest on Earth and Venus differs substantially (e.g.,
64 Wilson and Head, 1983; Wilson, 2009). For example, while the majority (*ca.* 90%) of Earth's
65 volcanism occurs along curvilinear belts and rift-margins, which collectively define tectonic plate
66 boundaries (Cottrell, 2015), Venus operates a stagnant-lid tectonic regime and is dominated by
67 features interpreted to be related to mantle plumes (e.g., Head et al., 1992). Although Venus is host
68 to volcanic features commonly observed on Earth, such as lava plains, discrete lava flows, shield
69 volcanoes, and shield fields, it is also home to enigmatic, flat landforms such as coronae (Head et
70 al., 1992; Stofan et al., 1992; Squyres et al., 1992; McKenzie et al., 1992; Grosfils and Head, 1994;
71 Addington, 2001; Krassilnikov and Head, 2003; Grindrod and Hoogenboom, 2006; Robin et al.,
72 2007; Wilson, 2009; Krassilnikov et al., 2012; Ivanov and Head, 2013).

73 An important difference between volcanism on Earth and Venus is that, by comparing intraplate
74 volcanic fluxes on both Earth and Venus, it is clear that Earth is the most volcanically active of the
75 two planets, possibly by an order of magnitude (Ivanov and Head, 2013). Indeed, while volcanic
76 activity on Earth is evidently abundant, evidence for ongoing, present-day volcanism on Venus is
77 comparatively sparse, although it is thought that the vast majority of the Venusian surface is
78 volcanic in origin (Head et al., 1992; Basilevsky and Head, 2003; Wilson, 2009). However, a
79 number of recent findings suggest that volcanic activity on Venus persists to the present: [1]
80 infrared radiation from three volcanic regions showed some flows to be warmer than their
81 surrounding rocks, implying that these lavas are younger than 2.5 Ma (Smrekar et al., 2010); [2]
82 sporadic atmospheric SO_2 fluctuations have been observed at Venus (Esposito, 1984; Marcq et al.,
83 2011); and [3] thermal spikes have been reported at Ganiki Chasma, a rift valley proximal to Ozza
84 and Maat Montes (Shalygin et al., 2015). In addition, the sulfuric clouds that envelop the entire
85 planet would not persist beyond 1–50 Ma without the replenishment of SO_2, the source of which is
86 presumed to be magmatic (Fegley and Prinn, 1989; Bullock and Grinspoon, 2001).

87 To emphasise the difference between volcanic activity on Earth and Venus: while Earth's oceanic

88 crust (that covers 60% of Earth's surface) has created >100,000 individual volcanoes (including
89 seamounts) in <100 Ma (e.g., Wessel et al., 2001 and references therein), Venus' entire surface has
90 produced roughly 70,000 individual volcanoes in <700 Ma (Head et al. 1992). The difference in the
91 rate of volcano production is therefore about an order of magnitude greater on Earth than on Venus.
92 We further note that, because >70% of all extrusive volcanism on Earth occurs beneath ocean
93 depths >1000 m under pressures >9 MPa, the presence coronae, a landform unique to the surface of
94 Venus, cannot simply be explained by the high Venusian atmospheric pressure (Smith, 1996). To
95 wit, Earth's ocean basins are not littered with coronae, but with well-formed stratovolcanoes (i.e.,
96 seamounts).

97 The principal goal of this contribution is to explore the reasons as to why Earth hosts vastly more
98 intraplate volcanoes than Venus. To do so, we formulate a conceptual model that combines data
99 from rock deformation experiments on basalts, which inform on the mechanical behaviour of the
100 crust and therefore the depth of the brittle-ductile transition (BDT) on both planets, with
101 atmospheric noble gas isotope data from Earth and Venus, which inform on planetary volcanic flux.
102 Additionally, our model also offers an explanation as to why volcanoes on Venus are
103 morphologically distinct from those on Earth.

104

105 **2 The deformation mode of the Terran and Venusian crusts**

106 The depth of the BDT on Venus has been estimated numerous times. For example, first-order
107 morphological differences between fold and thrust belts on Earth and Venus can be explained by a
108 shallow BDT on Venus relative to Earth (Williams et al., 1994). Spacing between adjacent
109 extensional structures may match the spacing between linear bands seen in the mountains of Ishtar
110 Terra on Venus if the surficial brittle layer is no more than a few km in thickness (Solomon and
111 Head, 1984). Preservation of substantial crater topographic relief on Venus is likely the result of a
112 thin (<10 km) brittle crust (Grimm and Solomon, 1988). Further, surface features within tesserae
113 (e.g., ribbons, long-wavelength folds, and grabens) offer a wealth of information as to the depth and

114 evolution of the BDT on Venus (Phillips and Hanson, 1998). For example, ribbons within tesserae
115 (Hansen and Willis, 1996) suggest a BDT as shallow as ~1 km during their formation (Hansen and
116 Willis, 1998; Ghent and Hansen, 1999; Ruiz, 2007). Of interest, long-wavelength folds and graben
117 are thought to reflect a deepening of the BDT over time (Phillips and Hanson, 1998)—but the depth
118 of the BDT during the formation of long-wavelength folds is estimated at only ~6 km depth (Brown
119 and Grimm, 1997; Ghent and Hansen, 1999). The pervasive deformation of the plateau highland
120 tesserae, the oldest preserved terrain, requires a weak, thin lithosphere (Brown and Grimm, 1999).
121 However, the presence of highland regions and large shield volcanoes (e.g., Crumpler et al., 1986;
122 Smrekar and Soloman, 1992; McGovern et al., 2014) implies localised crustal domains where the
123 BDT is deep enough to provide support for these structures. Nonetheless, these studies suggest that,
124 on average, the BDT on Venus is shallower than that on Earth.

125 We use here an experimental rock deformation approach to provide an alternate assessment for the
126 depth of the present-day BDT on Venus and Earth (see also Heap et al., 2017), which we interpret
127 here as a purely mechanical boundary between brittle and ductile behaviour. To do so, we compiled
128 experimental rock deformation data on basaltic (and diabase) samples deformed over a range of
129 confining pressures (analogous to depth) and temperatures (Table 1). We used these data to
130 construct a failure mode map that highlights the pressures and temperatures at which basaltic (and
131 diabase) rocks behave either in a brittle or a ductile manner in response to applied stress. We then
132 used this map to assess the position (depth) of the BDT on Earth and Venus. We first review some
133 important considerations for our experimental approach.

134

135 *2.1 Considerations for our experimental approach*

136 2.1.1 Composition of the Venusian crust

137 There is a dearth of *in-situ* quantitative geochemical data for Venusian surface rocks, and the
138 planet's thick CO_2-dominated atmosphere makes optical geological observations from orbit or

Earth-based telescopes impossible. The only available *in-situ* geochemical data from Venus are the major element composition of surface rocks, measured using gamma-ray and X-ray fluorescence spectroscopy. The three localities measured show basaltic compositions with SiO_2, FeO, MnO, and MgO abundances similar to mid-ocean ridge basalts on Earth (summarised in Bougher et al., 1997). Furthermore, the data from Venera 13 and 14 (Fe/Mg, Mg/Mn, K/U, and U/Th ratios) suggest Venus and Earth are made of the same chondritic material and have a similar internal structure, and that Venusian basalts are the product of similar degrees of partial (peridotite) mantle melting as those on Earth (Treiman, 2007; Hess and Head, 1990). Combined with the geomorphological data of Venus from radar imagery (i.e., reflectance spectra), it appears that most of the Venusian surface is volcanic in origin. This means the vast majority of the Venusian and Terran crusts are basaltic in their bulk composition (Basilevsky and Head, 2003). Therefore, we consider the deformation mode (i.e., brittle or ductile) of basaltic rocks collected on Earth to be analogous to the deformation mode of those on Venus.

2.1.2 Hydration of the Venusian crust

The Venusian atmosphere is extremely arid, with 150 times less H_2O compared with Earth's exosphere (Donahue and Russell, 1997). However, the lack of water in Venus' atmosphere and on its surface does not necessarily imply a desiccated crust. We suggest that the degree of hydration for Venusian crust and mantle (e.g., Kaula, 1990; Nimmo and McKenzie, 1996; Mackwell et al., 2008) requires re-examination. Note, the degassing of water is extremely inefficient for one-plate planets such as Venus or Mars. For example, it has been modelled that 90–95% of Mars' primordial water reserves should be retained in the mantle following accretion (Hunten, 1993), and recent data show the Martian mantle to be as 'wet' as the Terran mantle (McCubbin et al., 2012).

Combined, these studies conclude that substantial aqueous fluids can remain within planetary interiors, irrespective of the plate tectonic regime and without correlation to the degree of surface desiccation. For instance, if one were to distribute all of the water in the Earth's oceans into the

165 Venusian mantle, the water abundance (distributed in nominally anhydrous minerals) would not
166 exceed the storage capacity of a peridotitic mantle (Bell and Rossman, 1992; Kohlstedt et al., 1996;
167 Bolfan-Casanova et al., 2000; Lécuyer et al., 2000; Hirschmann, 2006; Smyth et al., 2006).
168 Furthermore, the Martian surface and atmosphere are both very water poor, but we know that the
169 crust on Mars is hydrated (Carr and Head, 2010; 2015). A volatile-rich interior on Venus (or at least
170 a hydrated mantle) could result in explosive volcanism (Thornhill, 1993; Fagents and Wilson, 1995;
171 Glaze et al., 2011; Airey et al., 2015), and some workers have proposed that some morphological
172 units on the Venusian surface are pyroclastic deposits (Campbell and Rogers, 1994; McGill, 2000;
173 Grosfils et al., 2011; Ghail and Wilson, 2013). Therefore, it is difficult to definitively conclude
174 whether the crust and upper mantle on Venus is desiccated or hydrous, and only future missions to
175 Venus can resolve this question. Because of this ambiguity, we contend that the consideration of all
176 of the available experimental rock deformation data for basalt and diabase (including the ultra-dry
177 diabase data from Mackwell et al., 1998) is an effective approach to investigate the failure mode of
178 rock within the Venusian crust. We also note that the majority of the basalts deformed in these
179 studies only contain a subordinate glass phase, if any. As a result, the impact of a glass phase,
180 hydrated or otherwise, should only play a very minor role in dictating the rheological behaviour of a
181 given sample (Smith et al., 2011; Violay et al., 2012; 2015).

182

183 *2.2 Determining the depth of the brittle–ductile transitions for Earth and Venus*

184 2.2.1 Essential nomenclature: brittle and ductile

185 Before interpreting the collated experimental rock deformation data it is important to outline some
186 essential nomenclature. The terms ‘brittle’ and ‘ductile’ are sometimes interpreted differently across
187 disciplines, which can cause confusion. To avoid such confusion, we define how we use these
188 terms.

189 Here, we use ‘brittle’ and ‘ductile’ to describe the failure mode of a rock sample on the lengthscale

of that sample (typically between 10 and 100 mm). Brittle behaviour is characterized by localised deformation, typically manifest as axial splits or shear fractures. During a deformation experiment, it is typical to observe an increase in porosity of a sample as the peak stress is approached. This increase in porosity is the result of the growth and formation of dilatant microcracks. Following a peak stress, a brittle experiment involves a stress drop (i.e., strain softening). This stress drop marks the point at which a macroscopic (i.e., across the lengthscale of the sample) fracture is forming or has formed—the hallmark of a brittle failure mode (see Hoek and Bieniawski, 1965; Brace et al., 1966; Scholz, 1968). We note that, in the case of highly porous samples, brittle deformation can be associated with a net decrease in porosity. In these cases, inspection of the post-deformation sample is required to verify the presence of axial splits or shear fractures.

We use the term ductility as per the definition of Rutter (1986), who described it as simply the capacity of a material to accommodate qualitatively substantial strain without the tendency to localise the flow into faults—localisation does not occur on the sample lengthscale. The concept of ductility is not dependent on the mechanism of deformation (Rutter, 1986). Although brittle behaviour is always the result of cracking on the microscale, ductile behaviour can be the product of a number of micromechanisms. For example, the micromechanism behind low-temperature, high-pressure cataclastic flow (i.e., ductile behaviour) is microcracking (Menéndez et al., 1996; Wong et al., 1997). Ductile behaviour typically involves the loss of porosity. We note that ductile behaviour can be associated with strain localization in certain circumstances: ductile behaviour in porous rocks can involve the formation of compaction bands (e.g., Baud et al., 2004) or bands of collapsed pores (e.g., Heap et al., 2015). The formation of such features is also associated with small stress drops in the mechanical data. In ambiguous cases, inspection of the post-deformation sample is required to verify the absence of axial splits or shear fractures, features synonymous with a brittle failure mode. Mechanical behaviour for two experiments is shown in Fig. 2, a typical brittle test and a typical ductile test (Violay et al., 2012; Heap et al., 2017).

2.2.2 Data selection

In the context of our study, we are interested in the transition between brittle behaviour and ductile behaviour as a result of viscous flow (i.e., the change in micromechanism from microcracking to viscous flow). We interpret viscous flow as non-recoverable viscoelastic deformation; this type of deformation is referred to as 'plastic' by some authors, but this term is sometimes also used to describe non-recoverable deformation in the brittle field. Since we are interested in the change in deformation micromechanism, we are not concerned here with low-temperature ductility driven by microcracking or cataclastic pore collapse, although very few studies exist on this topic for basaltic rocks (e.g., Shimada, 1986; Shimada et al., 1989; Adelinet et al., 2013; Zhu et al., 2016). We included all available experimental rock deformation data for basalt and diabase into our analysis (Table 1), with the exception of room-temperature experiments under uniaxial conditions (e.g., Al-Harthi et al., 1999; Heap et al., 2009; Schaefer et al., 2015), because they are of little use for determining the BDT, and those triaxial experiments that yielded non-viscous ductile behaviour such as cataclastic pore collapse (e.g., Shimada, 1986; Shimada et al., 1989; Adelinet et al., 2013; Zhu et al., 2016).

2.2.3 Limitations to our approach

One obvious limitation of our collation approach is that typical laboratory strain rates (~10^{-5} s^{-1}) are much faster than tectonic strain rates (e.g., Grimm, 1994). However, we recognise that [1] experiments already classified as ductile at laboratory strain rates will remain ductile at lower (i.e., natural) strain rates, and [2] lowering the strain rate at low experimental pressures and temperatures will reduce rock strength—because of the increased time available for subcritical crack growth (see Brantut et al., 2013 for a review)—but may not promote ductile deformation *per se*. For example, the experiments of Heap et al. (2011) showed that basalt can still fail in a brittle manner at a low laboratory strain rate of 10^{-9} s^{-1}. Although our approach utilises experiments conducted at high

241 strain rates, and so should be considered with this caveat in mind, our method does not assume a
242 representative basalt for the Venusian crust (see section 2.1 above).

243

244 2.2.4 Calculating depth

245 Each published experimental datum was assigned a failure mode: brittle or ductile, defined above.
246 Where necessary, and when possible, our definitions supersede those outlined in the studies from
247 which these data were collated. The effective pressure under which each experiment was performed
248 were converted to a depth with the relation $P = \rho \cdot g \cdot h$, where P is lithospheric or hydrostatic
249 pressure and g is surface gravitational acceleration, taken as 9.807 and 8.87 m/s^2 for Earth and
250 Venus, respectively. This approach allowed us to determine the lithostatic pressure gradients for
251 Earth and Venus. The bulk rock density, ρ, was determined with the following relation (Wilson and
252 Head, 1994):

253

254 $$\rho(h) = \frac{\rho_\infty}{[1 + \{V_0 - (1 - V_0)\} \exp(-\lambda \rho_\infty g z)]} \quad (1)$$

255

256 where ρ_∞ (the density of porosity-free rock) was taken as 2900 kg/m^3, V_0 is the void space fraction
257 (i.e., total porosity) at the surface (assumed here to be 0.25; see Wilson and Head, 1994), and the
258 constant λ was assumed to be 1.18×10^{-8} Pa^{-1} (Head and Wilson, 1992). Because of the very high
259 atmospheric pressure of Venus, the lithostatic pressure at the surface was taken as 9 MPa. The
260 hydrostatic pressure gradient for Earth was calculated using a constant water density of 1,000 kg/m^3
261 (yielding a pore pressure gradient of ~9.8 MPa/km). We note that the density of water does not vary
262 considerably at the pressures and temperatures relevant for the Earth's crust.

263 However, the nature of the pore fluid, and therefore the pore pressure gradient, for Venus is
264 enigmatic. The behavior of CO_2 at the atmospheric pressure and temperature of Venus is that of a

supercritical fluid and, if one assumes that supercritical CO_2 is a plausible pore fluid for Venus, the density will vary with pressure and temperature. For example, the density of CO_2 at the surface of Venus (at a pressure of 9 MPa and a temperature of 460 °C) is 65 kg/m^3. CO_2 density increases to 457 kg/m^3 at a pressure of 100 MPa and a temperature of 600 °C. Because of the relatively broad parameter space for pore fluid behaviour (and composition) on Venus, we considered three scenarios that likely capture the range of possible pore fluid densities within the Venusian crust. In one, the pore fluid had a constant density of 1,000 kg/m^3 (i.e., the same as on Earth, yielding a pore pressure gradient of ~8.9 MPa/km); in the second scenario, pore fluid had a density of 500 kg/m^3 and so a pore pressure gradient of ~4.4 MPa/km. In the third scenario, pore fluid density was 100 kg/m^3, giving a pore pressure gradient of ~0.89 MPa/km. In all cases, the pore pressure at the surface was taken as 9 MPa. In our analysis, we interpreted the pressure within the crust as the lithostatic pressure minus the pore fluid pressure.

2.2.5 Thermal gradients

Because we are discussing planetary-scale processes, we have opted to constrain the BDT on Earth using an average Terran geothermal gradient of 25 °C/km and an average surface temperature of 4 °C. Due to the lack of heat-flux measurements on Venus, all of the published thermal gradients are inferred. Importantly, as a result of the greenhouse effect imposed by an average atmospheric pressure of 9 MPa and a permanent cloud cover on Venus (Pollack et al., 1980), there is no meaningful difference in average surface temperature across the Venusian day–night cycle (where one Venusian day is equal to 116 Earth days) or with changes in latitude from the equator. In addition, since Venus has a hypsometry with a very low standard deviation (Fig. 1) there is an insignificant effect of altitude on the surface temperature when one considers a global average. Therefore, a representative surface temperature for Venus should have a small standard deviation from the assumed average value of 460 °C. To account for the uncertainty in the Venusian thermal gradient, we have used a selection of values from 5–40 °C/km (e.g., Sclater et al., 1980; Solomon

and Head, 1982; 1984; Grimm and Solomon, 1988; Burt and Head, 1992; Turcotte, 1993; 1995; Solomatov and Moresi, 1996; Turcotte et al., 1999; Leitner and Firneis, 2006).

2.2.6 BDT estimates for Venus and Earth using experimental data

Once the effective pressure of each experiment was converted to a depth, these data were plotted against the experimental temperature to examine the predicted depth of the present-day brittle–ductile transition on Earth (Fig. 3) and Venus (Fig. 4). The majority of experiments performed with basaltic rock samples were conducted under pressures equating to depths from 0 km (i.e., the surface) to 7 km (Shimada and Yukutake, 1982; Caristan, 1982; Bauer and Handin, 1983; Shimada, 1986; Duclos and Paquet, 1991; Schultz, 1993; Rocchi et al., 2004; Apuani et al., 2005; Benson et al., 2007; Ougier-Simonin et al., 2010; Heap et al., 2011, Violay et al., 2012; Adelinet et al., 2013; Violay et al., 2015; Schaefer et al., 2015; Zhu et al., 2016); few studies were performed under pressures corresponding to depths of up to 40 km (Griggs et al., 1960; Caristan, 1982; Hacker and Christie, 1991; Mackwell et al., 1998; Violay et al., 2012; 2015). In all cases, ductile behaviour was not observed below temperatures of 500 °C, even under an effective pressure of 500 MPa (e.g., Griggs et al., 1960). As expected, ductile behaviour is more commonly observed under combined high pressure and high temperature. Surprisingly, ductile behaviour was observed under room pressure (i.e., 0.1 MPa) at 800 °C (Figs. 3 and 4), which was likely the result of the presence of a melt phase; therefore, although these samples were of a basaltic bulk composition, they may not typify basaltic rocks. However, we prefer to retain all data for rocks of a basaltic composition in our analysis, for two reasons: first, not all of the experimental studies offer a detailed microstructural and compositional breakdown of their basaltic samples; second, we do not want to remove data based on our interpretation of what constitutes a basaltic rock typical of Venus or Earth.

Our analysis predicts that the BDT for the oceanic crust of Earth occurs at a depth of ~25-27 km (Fig. 3), consistent with the broad temperature-dependent (i.e., ~10–40 km depth) brittle–ductile transition predicted for a predominantly basaltic oceanic crust on Earth (Kohlstedt et al., 1995).

317 Assuming a pore fluid pressure gradient on Venus of ~8.7 MPa/km (Fig. 4a), we find that most of
318 the thermal gradients for Venus (i.e., 5–40°C/km) pass through a zone (from ~5 to ~18 km depth)
319 characterised by both brittle and ductile deformation. The difference in failure mode over this depth
320 interval arises from differences in rock properties such as composition, crystal size and content, and
321 porosity, as well as in factors such as strain rate (although we note that typically laboratory strain
322 rates rarely deviate from 10^{-5} s^{-1}). We interpret this depth interval on Venus as a failure mode
323 'transitional' zone. Below a depth of ~20 km, our collated experimental data predict exclusively
324 ductile behaviour when the thermal gradient is 15 °C/km or above for a pore pressure gradient of
325 ~8.7 MPa/km (Fig. 4a). However, this failure mode transitional zone is much shallower in the
326 (arguably more plausible) scenarios under which the Venusian pore pressure gradient is lower
327 (Figs. 4b and 4c). The failure mode transition zone on Venus exists at a depth of ~4–14 km (Fig.
328 4b) or ~2–12 km (Fig. 4c) for pore pressure gradients of ~4.4 or ~0.89 MPa/km, respectively.

329 Based on these collated experimental data, we conclude that the BDT occurs at a substantially
330 shallower depth on Venus than on Earth (when one considers global averages) (Figs. 3 and 4).
331 Therefore, these data show that although much of the crust on Earth behaves in a brittle manner, the
332 majority by volume of the Venusian crust should respond to stress in a ductile manner.

333

334 **3 Implications of a dominantly ductile crust on Venus**

335 *3.1 Implications for volcano morphology*

336 The tallest volcanoes on Earth, Venus, and Mars are intraplate volcanoes fed by deep-seated mantle
337 plumes (Head and Solomon, 1981; Donahue and Russell, 1997; Herrick et al., 2005; Wilson, 2009):
338 Mauna Loa on Earth (17.2 km of relief), Maat Mons on Venus (9 km of relief; Mouginis-Mark,
339 2016), and Olympus Mons on Mars (21.9 km of relief; Plescia, 2004), respectively). However,
340 shield volcanoes on Earth and Venus are dramatically different in terms of morphology: those on
341 Venus are, on average, wider and of lower elevation than those on Earth (700 km wide and 1.5 km

342 relief vs. 120 km wide and 8 km relief, respectively) (Head and Solomon, 1981; Head et al., 1992;
343 Herrick et al., 2005; Wilson, 2009). Because the loci of intraplate volcanism on Earth vary as
344 tectonic plates move across fixed mantle plumes, the maximum elevation of a volcano is therefore
345 not only supply limited, but is also constrained by the velocity of the plate (Morgan, 1971). By
346 contrast, Venus' stagnant-lid tectonic regime enables a volcano to grow for as long as the magma
347 source persists. Note, although it is debateable if plumes on Earth and Venus are geometrically
348 similar (Schubert et al., 1990; Stofan et al., 1995; Smrekar and Stofan, 1997; Jellinek et al., 2002;
349 Johnson and Richards, 2003; Ernst et al., 2007; Robin et al., 2007), the large shield volcanoes
350 observed on the Venusian surface are taken as evidence for long-lived mantle plumes in the
351 Venusian interior (Head and Solomon, 1981; Head et al., 1992; Herrick et al., 2005; Wilson, 2009).
352 With all else being equal, the average relief of shield volcanoes on Venus should therefore be
353 greater than their Terran counterparts (Wilson, 2009). But, other than some rare if notable
354 exceptions (e.g., Maat and Skadi Montes), Venusian volcanoes are not higher in relief than their
355 Terran counterparts. To explore this discrepancy we assess here three first-order variables that we
356 consider important in controlling the elevation of a volcanic construct: [1] surface gravity, [2] the
357 viscosity of extruded lavas, and [3] the flexural response of the lithosphere to geological loads.

358

359 3.1.1 Surface gravity

360 Mars is host to the largest volcanoes in the Solar System. This is, in part, because high-relief
361 structures are easier to build and retain on Mars because of its relatively low surface gravity (i.e.,
362 3.71 m/s^2, compared with 9.81 m/s^2 and 8.81 m/s^2 on Earth and Venus, respectively) (Heap et al.,
363 2017). However, the surface gravitational acceleration on Venus is very similar to that of Earth
364 meaning that, if all else were equal, both planets should extrude lava flows of a similar thickness
365 and build shield volcanoes of a similar size over a given timescale. Large basaltic flows on Earth
366 are typically <30 m thick, and—again, because of the comparable surface gravitational
367 accelerations of Earth and Venus—the same should be true for Venus. This inference is consistent

with radar imaging of Venus that shows that flows rarely exceed the vertical resolution of the Magellan topographic data (which has a height resolution of 5-50 m; e.g., Pettengill et al., 1991; Roberts et al., 1992; Wilson, 2009). We conclude therefore that the minor difference in surface gravity between Earth and Venus cannot explain the considerable contrast in volcano relief.

3.1.2 Viscosity of extruded lava flows

On Earth, high-viscosity lavas are better able to construct a tall volcanic edifice than low-viscosity lavas, which tend to travel much greater distances from the vent (e.g., Harris and Rowland, 2009). Although the bulk composition of Earth and Venus are similar (Bougher et al., 1997), the substantial influence of water content on the viscosity of melts (e.g., Dingwell et al., 1996) means that if Venusian melts are anhydrous (dry) then the lavas erupted onto its surface should have a higher viscosity than their Terran counterparts. It is possible that the Venusian mantle is about an order of magnitude more viscous than that of Earth, based on the assumption that Venusian melts are anhydrous and derived from an anhydrous mantle (Kaula, 1990; Nimmo and McKenzie, 1996; Mackwell et al., 1998). However, and as outlined above, recent data that suggest a hydrated Martian mantle (McCubbin et al., 2012) demand a reappraisal of the assumption that the Venusian mantle is anhydrous. Indeed, the vast majority of basaltic lava flows on the Venusian surface are of a similar spatial magnitude and thickness to the flows observed in basaltic large igneous provinces (LIPs) on Earth (e.g., Columbia River and Deccan Traps; Wilson, 2009); this similarity, together with the similar surface gravity of Earth and Venus, implies a similar basaltic flow viscosity. We also note that an increase in temperature results in a decrease in melt viscosity (Hess and Dingwell, 1996; Giordano et al., 2008), even for anhydrous melts (Hess et al., 2001). Therefore, if Venusian lavas are indeed anhydrous, the high temperature of the Venusian surface may decrease their nominal eruptive viscosity to a value closer to lavas extruded on Earth. We conclude, therefore, that the difference in viscosity of erupted lavas cannot explain the difference in morphology between the volcanoes on Earth and Venus.

3.1.3 Response of the lithosphere to geological loads

An additional parameter that controls the height of a volcanic structure is the mechanical rigidity of the basement upon which the volcano is situated (Watts, 2001). The flexural rigidity of the lithosphere depends on its rheology such that a strong and brittle lithosphere is better adapted to support high-elevation structures than a weak and ductile lithosphere (Watts, 2001). Indeed, a thick and predominantly brittle crust has been used to explain the presence of the ultra-high-elevation volcanoes on Mars (Turcotte et al., 1981; Heap et al., 2017), with the mechanical response of the Martian crust even influencing the eruptive behaviour of these shield volcanoes (Byrne et al., 2013).

We contend that the experimental rock deformation data collated in Figs. 3 and 4 provide a simple explanation as to why Venus hosts volcanoes that, although perhaps as voluminous, are wider and of lower elevation than those on Earth. On a global scale, high-elevation structures cannot be supported on Venus to the same extent as they are on Earth due to the dominantly ductile Venusian crust. Recent analogue modelling by Byrne et al. (2013) aligns with this conclusion. This prediction further suggests that the volcanic topographic highs on Venus (e.g., Maat Skadi Montes) may be relatively young, because our model predicts that high-elevation structures on Venus will force the underlying lithosphere to yield over geological timescales (according to the models presented by Byrne et al. (2013); see also Smrekar and Solomon (1992) and Herrick et al. (2005)). Large volcanoes may even evolve into corona-like structures over time, evidenced by the number of volcano-corona 'hybrids' on the Venusian surface (e.g., Atai Mons; Grindrod et al., 2006). We also note that the downflexing of the lithosphere beneath a volcano imposes a constrictional strain upon the edifice, manifest as imbricate shortening structures arrayed around its flanks (Byrne et al., 2009; 2013). Unfortunately, the flanks of Venusian volcanoes are not sufficiently resolved with currently available data to test this hypothesis (full resolution Magellan topographic imagery has a resolution of about 100 m; Herrick et al., 2005).

3.2 Implications for volcanic character

The dominant mode of magma migration through Earth's crust (in terms of volume) is via fractures (e.g., Gudmundsson, 2006). The experimental data collated here suggest that, on Venus, faulting could be restricted to shallow depths (i.e., 2–12 km) (Fig. 4). Similar to Earth (Burov and Gerya, 2014), a rising mantle-derived melt on Venus will pond and spread laterally, underplating the crust at depths greater than that of the BDT (as shown in Fig. 5 a-c for Venus). However, based on our depth estimates for the BDT on Venus (Fig. 4), the mechanism by which magmas on Venus can continue to migrate towards the BDT is through buoyancy-driven diapirism. Importantly, however, the lengthscale for magma migration by diapirism is considerably shorter than migration through dykes (Rubin, 1995; Gudmundsson, 2002; Petford, 2003; Gudmundsson, 2006; 2011) and diapirs will inevitably pond and create sills due to a stress-related equilibrium when the forces driving ascent are equal (or less than) the forces acting against ascent (i.e., crystallisation increasing viscosity) – unless more magma is added to further drive ascent via buoyancy-driven diapirism. Therefore, if magma transport through the lower to middle Venusian crust is dominated by diapirism, then a lower fraction of crust-situated melt can reach the surface and erupt, relative to Earth. Occasionally however, a sill may form that is large enough to generate enough uplift to initiate faulting in the brittle crust, creating a set of concentric vertical faults (see Galgana et al., 2013). If the magma reaches these faults (or vice versa) then melts can propagate upwards, forming ring-dikes or arachnoids (Head et al., 1992; Donahue and Russell, 1997; Basilevsky and Head, 2003; Wilson, 2009). Should it reach the surface, this melt will erupt as lava, and we conceptually show how this can result in the formation of the curious coronae features on Venus in Fig. 5.

A combination of lateral flow and dyke-facilitated volcanism will cause the sill (magma chamber) to contract vertically, and this can cut off the magma supply to the surface as the collapsing brittle crust closes the fracture network. This may result in subsidence beneath the forming or formed coronae with either negative or positive relief (both of which are commonly observed on Venus: Head et al., 1992; Donahue and Russell, 1997; Basilevsky and Head, 2003; Herrick et al., 2005;

446 Wilson, 2009), which we argue is the result of variable ratios of the erupted lava to the amount of
447 subsidence. If the magma supply from the plume to the crust is large enough and is active over
448 sufficient timescales, then a shallow-flanked shield volcano could form (e.g., Maat Mons), the
449 vertical growth of which is likely tempered by the inability of the predominantly ductile Venusian
450 crust to support high-elevation structures (due to its low flexural rigidity). However, if the magma
451 chamber (sill) cannot connect with the faults, because the sill has stalled below the BDT, then
452 surface eruption will not ensue. In this eventuality, grabens (*fossae* and *lineae*), fractures, scarps
453 (*rupes*), or troughs will form, tectonic landforms common to the Venusian surface (Head et al.,
454 1992; Donahue and Russell, 1997; Basilevsky and Head, 2003; Wilson, 2009).

455 Most volcanic systems on Earth show complex magmatic plumbing with several reservoirs situated
456 at different depths. However, most primary mantle melts that reach the Earth's crust form sill-like
457 magma chambers at the base of the crust (defined as primary magma chambers) and are typically
458 found at depths considerably greater than 10 km (Kelley and Barton, 2008; Stroncik et al., 2009;
459 Becerril et al., 2013). Therefore, on Earth, most shallow magma chambers are connected to a deeper
460 primary magma chamber at depths of >10 km (Hill et al., 2009; Michon et al., 2015). This magma
461 system architecture suggests that magma ponds at the crust–mantle boundary on Earth. Therefore, if
462 Venusian melts form magma chambers at similar depth, or at a similar depth with respect to the
463 stratigraphy of the crust (i.e., the crust–mantle boundary), as predicted for shallow magma
464 chambers (Wilson and Head, 1994), then those chambers will be hosted below the BDT (predicted
465 to occur between 2 and 12 km on Venus: see Fig. 4a-c), restricting magma mobility to the short
466 lengthscales typical of diapirism (Rubin, 1995; Gudmundsson, 2002; Petford, 2003; Gudmundsson,
467 2006; 2011).

468 We can therefore predict, albeit qualitatively, that a greater proportion of magmatism on Venus
469 does not result in volcanism, but instead results in plutonism, than on Earth. Indeed, lava flow unit
470 thickness estimates from Magellan topographic data suggest that coronae are probably underlain by
471 large magma bodies that are not emptied during eruption (Grindrod et al., 2010). Any crustal

thickening in areas of high magmatic activity should thus be compensated by delamination back into the mantle with or without crustal uplift (Smrekar and Stofan, 1997; Ghail, 2015). To test the hypothesis that plutonism is favoured over volcanism on Venus (relative to Earth), we will now compare differences in volcanic flux on Earth and Venus with the available geochemical data.

4 Measuring the volcanic eruptive flux of Venus and Earth

Finding a suitable metric to compare the eruptive fluxes of Venus and Earth is challenging. For example, there is a large uncertainty for both the longevity and frequency of Venusian volcanism due to the lack of reliable chronostratigraphic or radiogenic isotopic data for the Venusian surface (Head et al., 1992; Basilevsky et al., 2003; Kreslavsky et al, 2015). However, there is evidence that Venus has experienced some voluminous volcanism in the past, coined 'global resurfacing events'. The model for catastrophic volcanic resurfacing is based on the relatively few (*ca.* 1,000) impact craters, and is thought to have occurred between 300 Ma and 1 Ga (e.g., McKinnon et al., 1997). Assuming a frequency of resurfacing episodes that declined with the rate of heat generation (based on K–Th–U systematics of the mantle), Kaula (1991) proposed that there could have been eight resurfacing events over Venus' 4.56 Ga history. Volcanism on Venus appears to be mostly quiescent between these resurfacing events, which are either random or occurring roughly once every 0.5 Ga (Kaula, 1991). If in fact magmatism during these largely passive periods does not result in extrusive volcanism, then by our inference it may instead be manifest as massive magmatic underplating of basaltic melts at the base of the crust and subsequent plutonism in the crust, possibly followed by delamination back into the mantle (Smrekar and Stofan, 1997).

An important and poorly constrained parameter is the thermal structure of the Venusian interior. Nimmo and McKenzie (1997; 1998) cite the composition (specifically the FeO abundance) of the basaltic rocks analysed by the Venera and Vega landers to argue that the potential temperature of the Venusian mantle was similar to the Earth's during the emplacement of these rocks. Note, the FeO data used by Nimmo and McKenzie (1997; 1998) are by no means absolute or accurate (they

498 have large uncertainties), but this is the only data presently available and future missions are
499 required to provide an improved insight. Nevertheless, they do provide a quantitative model with
500 which to demonstrate the point. Since these basalts are between 300–800 Ma one must calculate the
501 mantle temperature for the present day; this is because resurfacing events would have cooled the
502 Venusian upper mantle, which would have been followed by an increase in temperature due to U–
503 Th–K decay and thermal insulation by the crust. Nimmo and McKenzie (1997, 1998) concluded
504 that it is unlikely that the Venusian mantle increased in temperature by more than 200 °C over 800
505 Ma. Hence, these workers proposed an upper limit of 1500 °C for the potential temperature of the
506 present-day Venusian mantle (Nimmo and McKenzie, 1998). This temperature is below the solidus
507 for water-undersaturated peridotite (Kohlstedt et al., 1996; Hirschmann, 2006), and so melt
508 production would be restricted to adiabatic melting of thermochemical plumes rising through the
509 mantle (e.g., such as the Hawaiian plume on Earth; Morgan, 1971).

510 A key feature of the conceptual model presented here is that, all else being equal, the volcanic
511 eruptive flux of Venus should be lower than that of Earth. Since we cannot rely on estimates of
512 volcanic flux from chronostratigraphic methods, we must look elsewhere. For example, the
513 chemistry of a planet's atmosphere is a passive recorder of surface and subsurface processes –
514 including volcanism (e.g., Mather, 2008; Gaillard and Scaillet, 2014; Mikhail and Sverjensky,
515 2014). Therefore, if Venus has experienced a relatively retarded volcanic eruptive flux (relative to
516 Earth) over its geological history then this will have left a geochemical fingerprint in the chemistry
517 of the Venusian atmosphere. Herein therefore we focus on the stable isotopes of argon, principally
518 ^{36}Ar, ^{38}Ar, and ^{40}Ar, as useful tools for investigating the origin of volatiles (with ^{38}Ar/^{36}Ar) and the
519 degassing history (with ^{40}Ar/^{36}Ar) of Venus. This is because [1] there are data for the ^{40}Ar/^{36}Ar and
520 ^{38}Ar/^{36}Ar ratios for the atmospheres of Earth, Mars, Venus, and solar wind (Porcelli and Pepin,
521 2002), and [2] ^{36}Ar and ^{38}Ar are primordial isotopes whereas ^{40}Ar is produced from the decay of
522 ^{40}K, with a half-life of 1.25 Ga, meaning that ^{40}Ar in planetary atmospheres can be used to derive
523 information regarding the degassing of planetary interiors (e.g., Halliday, 2013).

5 Validating the model: argon isotope data

Despite the dearth of missions into and below the Venusian atmosphere over the past 40 years, there are valuable data for the major and minor element geochemistry of the Venusian atmosphere, including argon isotope ratios. Indeed, argon isotopes have been previously used to inform on the evolution of Venus (e.g., Istomin et al., 1980; Hoffman et al., 1980a, b; Turcotte and Schubert, 1988; Kaula, 1990; 1991; Namiki and Solomon, 1998; Porcelli and Pepin, 2002; Mikhail and Sverjensky, 2014; Halliday, 2013; O'Rourke and Korenaga, 2015).

In December 1978, seven gas analysers (four mass spectrometers and two gas chromatographers) provided *in-situ* measurements of the Venus atmospheric chemical and isotopic composition (summarised by Hoffman et al., 1980a). The Soviet Union's Venera 11 and 12 landers (Istomin et al., 1979) and the United States Pioneer Venus entry probe (Hoffman et al., 1980a) determined the argon isotope composition of the lower Venusian atmosphere (below the altitude limit of isotopic homogenisation). Importantly, these two independent measurements provided a $^{38}Ar/^{36}Ar$ ratio within error of one another (summarised by Hoffman et al., 1980b). The similarity for the $^{38}Ar/^{36}Ar$ ratios for Earth and Venus is indicative of a shared source of volatile elements (Fig. 6). We consider that the most surprising result of these measurements was that the ratio of radiogenic to primordial argon in the Venusian atmosphere was shown to be highly unradiogenic, with a $^{40}Ar/^{36}Ar$ ratio of only 1.03 ± 0.04. For comparison, most argon in the atmospheres of Earth and Mars is strongly radiogenic, with $^{40}Ar/^{36}Ar$ ratios of 298.56 and 1900 ± 300, respectively (Fig. 6). Below, we outline why atmospheric loss, Venus being a K-deficient planet, and diffusive degassing cannot explain the difference between the $^{40}Ar/^{36}Ar$ ratios of Earth and Venus. We then finish by proposing a solution (that leans on the notion of a shallow BDT for Venus), where we conclude that this discrepancy can be explained by a relatively low volcanic eruptive flux for Venus (compared to Earth).

549 *5.1 The case against atmospheric loss to explain the unradiogenic argon*

550 One of the principle mechanisms leading to stable isotope fractionation of atmosphere-forming
551 elements is low-temperature atmospheric loss (i.e., hydrodynamic escape). This process induces
552 mass dependant stable isotope fractionation, and therefore preferentially removes the lighter
553 isotopes over the heavy isotopes (e.g., ^{36}Ar over ^{38}Ar, and ^{38}Ar over ^{40}Ar). This, in turn, means that
554 the ^{38}Ar/^{36}Ar ratio would reflect substantial stable isotope fractionation if atmosphere loss to space
555 were the sole reason for the unradiogenic ^{40}Ar/^{36}Ar ratio in the Venusian atmosphere. Note, this is
556 not the case for the Venusian and Terran datasets (Fig. 6). Hydrodynamic escape of ^{36}Ar cannot
557 explain the low ^{40}Ar/^{36}Ar ratio of the Venusian atmosphere, because the ^{36}Ar/^{38}Ar data for the
558 Venusian and Terran datasets are almost identical (i.e., 5.5 vs. 5.3; see Fig. 6), and Earth and Venus
559 have very similar escape velocities for argon (*ca*. 12 and 13 km/s, respectively). Because Earth and
560 Venus both show primordial ^{36}Ar/^{38}Ar ratios, both planets appear to share identical (isotopic) source
561 materials (i.e., both are similar to their initial value recorded by solar wind: Porcelli and Pepin,
562 2002; Halliday, 2013). This in turn implies that both Earth and Venus had the same initial
563 atmospheric ^{40}Ar/^{36}Ar ratio. A conundrum thus ensues: where is the missing ^{40}Ar in the Venusian
564 atmosphere?

565

566 *5.2 The case against Venus being a K-deficient planet*

567 The unradiogenic ^{40}Ar/^{36}Ar ratio for the Venusian atmosphere also cannot be explained by
568 proposing Venus to be a K-deficient planet, because the average observed K/U ratio in rocks on the
569 Venusian surface is 7,220 (akin to mid-ocean ridge basalts on Earth). Therefore, assuming an initial
570 K/U and ^{38}Ar/^{36}Ar ratio for Earth and Venus, the present-day ^{40}Ar/^{36}Ar ratio of the Venusian
571 atmosphere is not a reflection of the overall K abundance, but would therefore reflect either the flux
572 of ^{40}Ar diffused or degassed out of the mantle and/or crust.

573

574 *5.3 The case against efficient, diffusive degassing*

575 The efficient transport of ^{40}Ar from the interior of a planet into its atmosphere can be, conceptually,
576 achieved by diffusion. The entire Venusian crust is at a temperature above the closure temperature
577 for argon in most silicate systems (Kelley and Wartho, 2000). However, efficient (or total) diffusion
578 of ^{40}Ar through the crust cannot be proposed, because the Venusian atmosphere is strongly
579 unradiogenic (for argon). This indicates that the Venusian crust has retained considerable ^{40}Ar
580 produced continually over the age of the planet (4.56 Ga). The BSV must therefore be saturated in
581 ^{40}Ar. The lack of ^{40}Ar-diffusion at high Venusian surface temperatures can be explained by the lack
582 of a chemical gradient. A buildup of ^{40}Ar in the crust above the closure temperature does not
583 necessarily mobilize the ^{40}Ar into the atmosphere. Buoyancy drives ascent, but pathways and
584 mobilising agents are also required (note, gravity and physical inhibition are also acting as opposing
585 forces). The lack of ^{40}Ar transport can be explained by a system that rapidly reaches equilibrium
586 with the intergranular medium, despite diffusion coefficients great enough to model efficient
587 mobilisation, conceptually (Cassata et al., 2011), Furthermore, mass-transfer along the grain
588 boundary of silicates and oxides is limited to a very thin layer (*ca*. 1 nm; Joesten, 1991), so the bulk
589 diffusivity should be reduced by the ratio of the thickness of the grain boundary to the diameter of
590 the grain (Faver and Yund, 1992). For a grain diameter of 0.1 to 1 mm, the diffusive lengthscales of
591 argon is <1.2 km in 1 Ga. Since the lengthscale is less than the likely thickness of the Venusian
592 crust (which is most certainly >1.2 km), the nominal diffusive flux of ^{40}Ar to the atmosphere is
593 effectively zero over 1 Ga (Namiki and Solomon, 1998). Therefore, the nominal diffusive flux of
594 ^{40}Ar to the atmosphere will be negligible over 4.5 Ga.

595

596 *5.4 The case for a low volcanic eruptive flux on Venus relative to Earth*

597 We propose volcanism is the main liberating agent for transporting ^{40}Ar to the Venusian
598 atmosphere. During mantle melting on Earth and Venus, ^{40}K and ^{40}Ar are mobilised in melts,
599 because they are both incompatible elements in primary mantle silicates, e.g., olivine (Chamorro et

al., 2002; Brooker et al., 2003). This degassing implies that the strongly unradiogenic low $^{40}Ar/^{36}Ar$ ratio in the Venusian atmosphere is mirrored by a higher crustal excess of ^{40}Ar than is observed for the crust on Earth (which is known to contain excess ^{40}Ar: Allègre et al., 1996; Kelley, 2002). We argue that most of the ^{40}Ar transported in melts from the Venusian mantle is locked in plutons and stored within the Venusian crust, implying that there is a large excess of ^{40}Ar in the BSV. Our contention that a dominantly ductile Venusian crust (Fig. 4a-c) inhibits volcanism but results in abundant plutonism (relative to Earth; Fig. 7) forms a testable hypothesis: Venus should have degassed less ^{40}Ar, relative to Earth. Mars, for example, has a highly fractionated $^{36}Ar/^{38}Ar$ ratio of 4.1 (Porcelli and Pepin, 2003; Halliday, 2013), which reflects a substantial low-temperature loss of its atmosphere (Porcelli and Pepin, 2003; Halliday, 2013) (Fig. 6). Consequently, their present-day atmospheric $^{40}Ar/^{36}Ar$ ratios will reflect their relative efficiencies in ^{40}Ar degassing. The present-day Venusian atmosphere has a strongly unradiogenic $^{40}Ar/^{36}Ar$ ratio of 1.03 ± 0.04, compared with 298.56 for Earth (Kaula, 1991; Porcelli and Pepin, 2003; Halliday, 2013). However, the Venusian atmosphere also contains roughly two orders of magnitude more ^{36}Ar relative to Earth's atmosphere (Porcelli and Pepin, 2003). If we correct the $^{40}Ar/^{36}Ar$ ratio for Venus then the $^{40}Ar/^{36}Ar$ ratio of the Venusian atmosphere would be approximately 103, meaning Earth has degassed three times more ^{40}Ar than Venus. We view this implication here as a consequence of a higher rate of volcanism on Earth than on Venus. This is because the majority of Earth's volcanism is directly related to Earth's mobile-lid plate tectonic regime (Cottrell, 2015), but we argue that the high surface temperature and dearth of deep crustal faults on Venus also plays an important role. Therefore plutonism, rather than volcanism, is the dominant mode of magmatic activity on Venus (Fig. 7) and this is reflected in the unusually unradiogenic $^{40}Ar/^{36}Ar$ ratio observed in the Venusian atmosphere (Fig. 6).

6 Concluding remarks

We present here an experimentally-constrained and isotopically-supported conceptual model that predicts Venus to have been less volcanically active relative to Earth by a factor of three, in terms

626 of eruptive flux. Since the volume of magma erupted cannot be directly discussed, we focus here on
627 the degassing flux constrained by argon isotopes, which show that Earth has degassed three times
628 more ^{40}Ar than Venus. We conclude that the reduced eruptive flux on Venus, compared to Earth, is
629 the result of the hot Venusian climate, a factor that greatly impacts the dominant failure mode of,
630 and therefore the method by which magma can travel up through, the Venusian crust. The higher
631 rate of intraplate volcanic activity on Earth is exemplified by the observation that Earth's relatively
632 young oceanic crust has seen the development of <100,000 individual volcanoes (i.e., seamounts) in
633 <100 Ma, whereas Venus has only produced *ca*. 70,000 individual volcanoes over a much longer
634 time period (700-1000 Ma) – a difference of an order of magnitude.

635 An interrogation of high pressure, high temperature experimental rock deformation data suggests
636 that the unrelenting high temperature (460 °C) of the Venusian surface modifies the rheology of the
637 Venusian crust such that the dominant failure mode within the Venusian crust is ductile. These data
638 highlight that the BDT on Venus could be as shallow as 2–12 km (Fig. 4), while the same method
639 yields a realistic estimate for the BDT on Earth of ~25-27 km (Fig. 3). The implications of a
640 dominantly ductile Venusian crust are twofold. First, the flexural rigidity of the Venusian
641 lithosphere will be low, inhibiting the formation of high-relief volcanoes (via lithospheric flexure).
642 We further note that the low flexural rigidity of the Venusian lithosphere may not just impact
643 volcano morphology, but also the global hypsometric profile of Venus (Fig. 1). We therefore
644 speculate that the low standard deviation of the Venusian surface is also the consequence of its hot
645 climate. Second, magma delivery to the surface through fractures (i.e., dykes)—the dominant
646 transport mechanism of magma to shallow crustal levels on the telluric planets (e.g., Wilson and
647 Head, 1994; Gudmundsson, 2006)—will be impeded on Venus. Our conceptual model therefore
648 predicts that most magma on Venus will stall in the crust as sills, rather than be erupted at the
649 surface: plutonism, rather than volcanism, is the dominant mode of magmatic activity on Venus
650 (Fig. 7). Importantly, these implications are supported by the atmospheric argon isotope ratios for
651 Earth and Venus, which indicate that volcanic degassing, and therefore volcanic flux, has been three

times lower on Venus than on Earth over the past 4.5 Ga (Fig. 6).

Our conceptual model falls short in describing, for example, the formation histories for the Venusian continents, Aphrodite Terra and Ishtar Terra (which, speculatively, could be the result of isostatic rebound before the global resurfacing event, or crustal delamination of the lower lithosphere back into the mantle, or a presently unknown mechanism; Smrekar and Stofan, 1997; Ghail, 2015). We also highlight that our conceptual model assumes various similarities between Earth and Venus, such as similar mantle convective regimes, which may not be strictly true (e.g., Johnson and Richards, 2003; Robin et al., 2007). Nevertheless, our model offers a viable explanation for the difference in volcano morphology between Earth and Venus (i.e., the presence of coronae) and the relative quiescence of volcanism on Venus compared to Earth (i.e., the order of magnitude difference in the rate of intraplate volcano formation between Earth and Venus). Furthermore, a Venusian BDT as shallow as predicted here also implies that faulting through the vertical lengthscale of the crust is hindered. Therefore, the hot climate of Venus may also inhibit the formation of the plate tectonic boundaries that sub-divide the crust (Foley et al., 2012; Bercovici and Ricard, 2014). Our study highlights another example of the complex interplay between climate and geodynamics.

Acknowledgements

We acknowledge stimulating discussions on argon geochemistry with Simon Kelley, Chris Ballentine, Colin Jackson, and Peter Barry, and with Richard Ghail on the tectonic history of Venus. We also acknowledge critical comments by Nicolas Le Corvec, Paul Byrne, two anonymous reviewers, and the editorial handling of Mark Jellinek that enabled us to improve this manuscript. M.J. Heap acknowledges funding from an Initiative d'Excellence (IDEX) "Attractivité" grant (VOLPERM), funded by the University of Strasbourg. All of the data used in this manuscript are cited in the reference list.

677

678 **Figure captions**

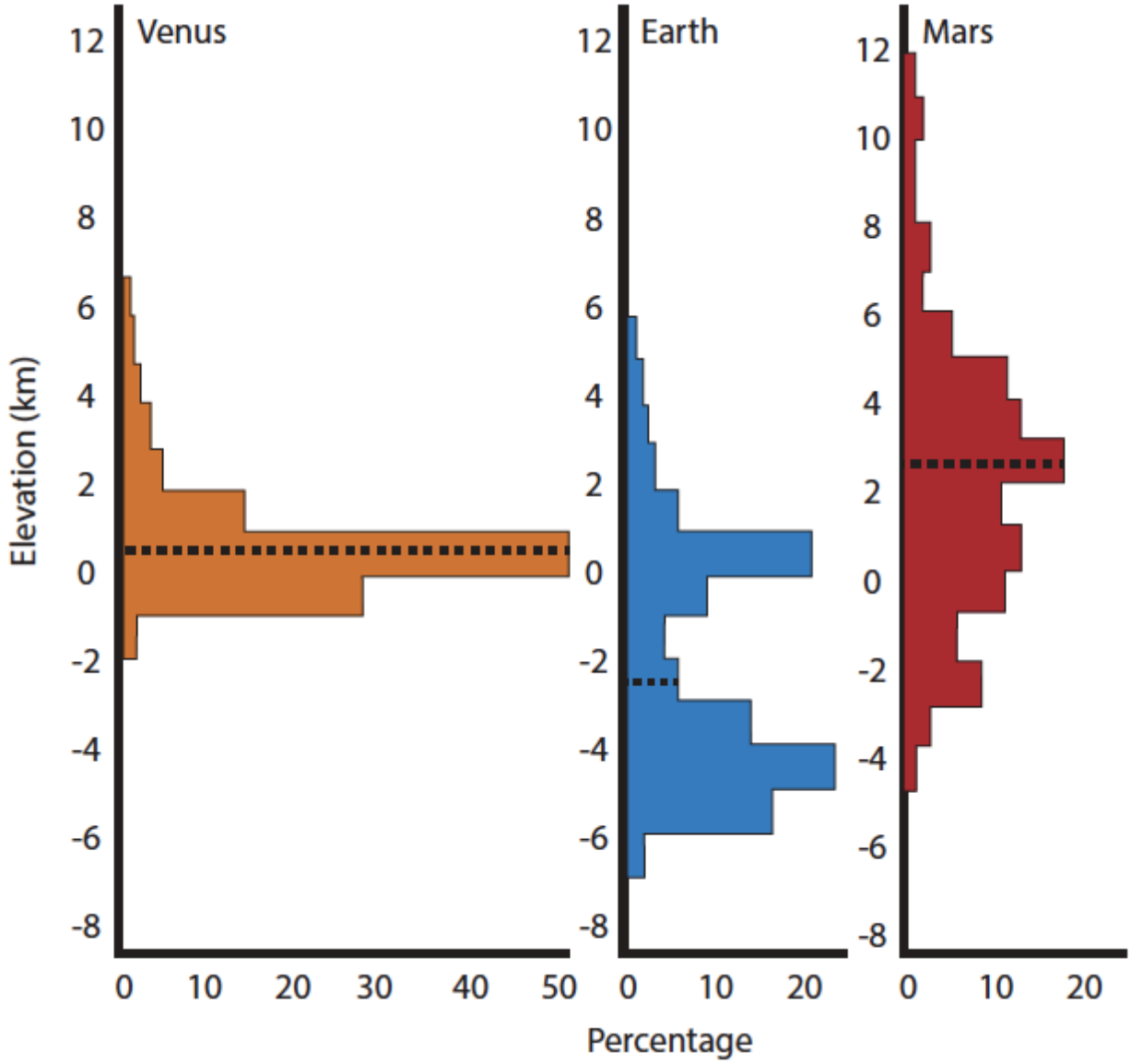

679

680 **Fig. 1**: Hypsography of Venus, Earth, and Mars (Head and Solomon, 1981; Basilevsky and Head,

681 2003; Taylor and McLennan, 2009). Dashed lines mark the mean surface elevation for each planet.

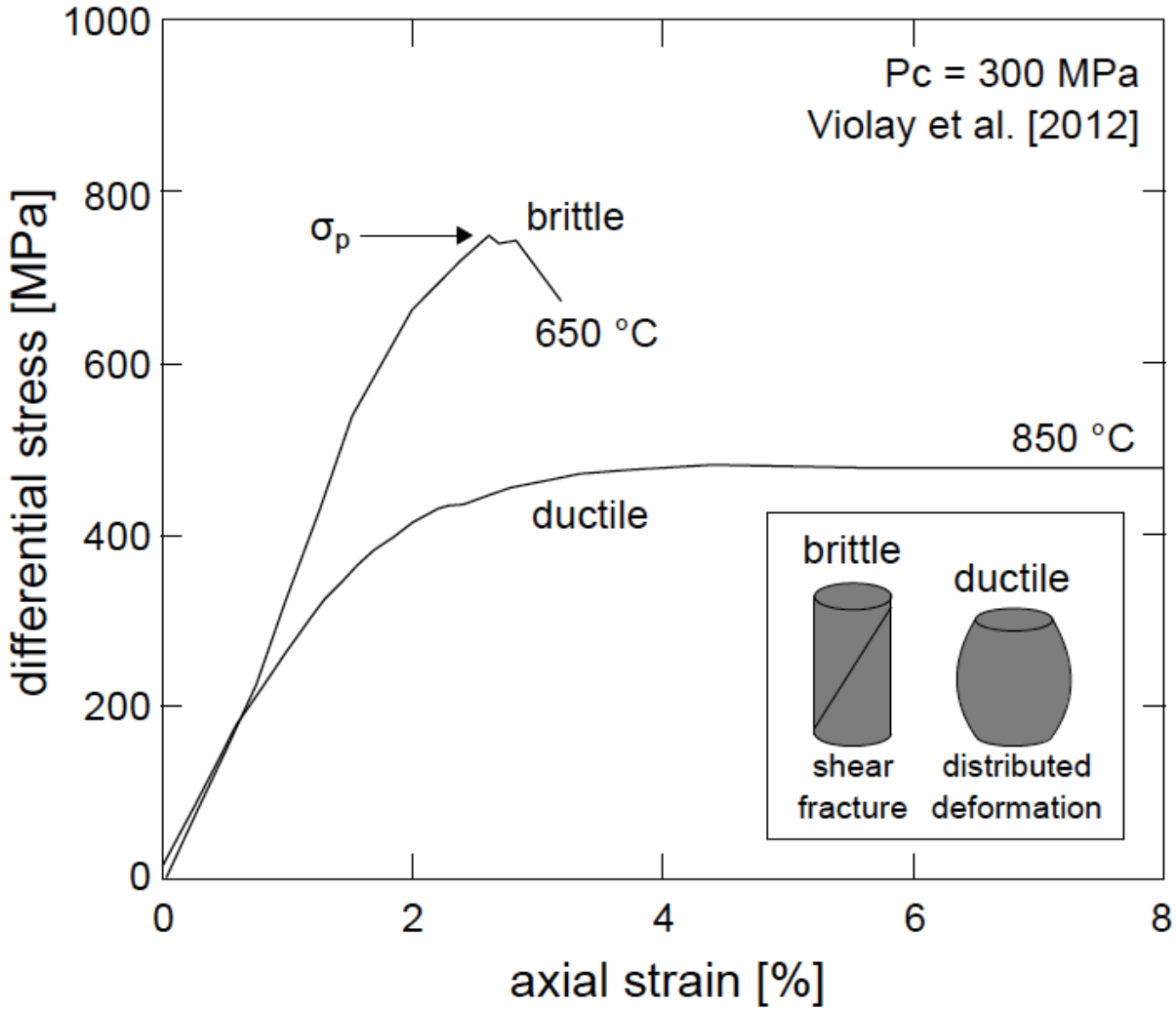

682

683 **Fig. 2**: The mechanical behaviour of rock in compression (from Heap et al., 2017). Examples of
684 brittle and ductile stress-strain curves for basalt deformed at a confining pressure of 300 MPa and a
685 temperature of 650 °C (brittle test) and 850 °C (ductile test) (data from Violay et al., 2012). Inset
686 shows cartoons depicting post-failure samples typical of brittle (throughgoing shear fracture) and
687 ductile (distributed deformation) deformation.

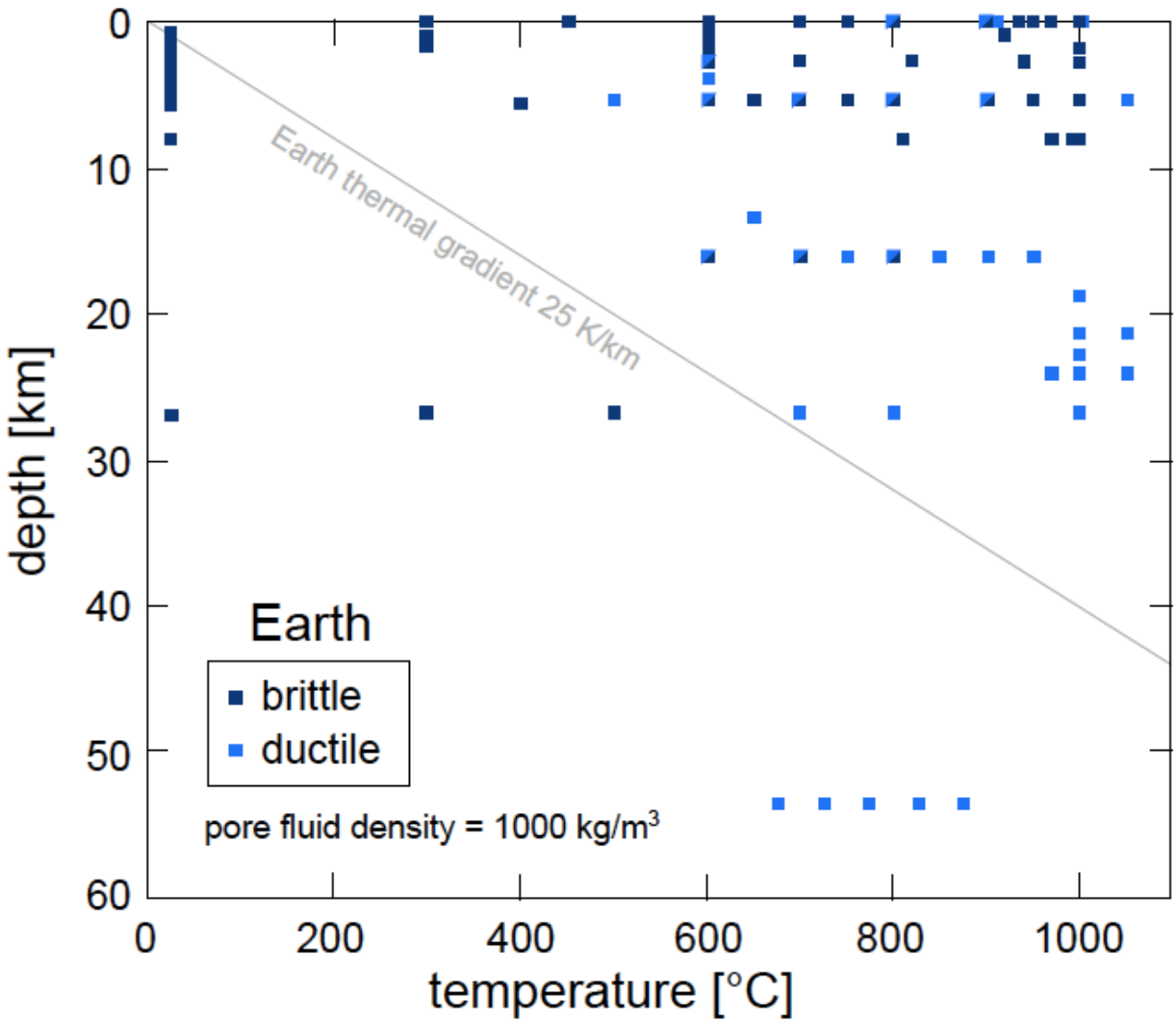

688

689 **Fig. 3**: Failure mode map (brittle or ductile) for Earth assuming a pore pressure gradient of ~9.8
690 MPa/km, a surface gravity of 9.807 m/s^2, an average thermal gradient of 25 °C/km, and an average
691 surface temperature of 4 °C. See text for details.

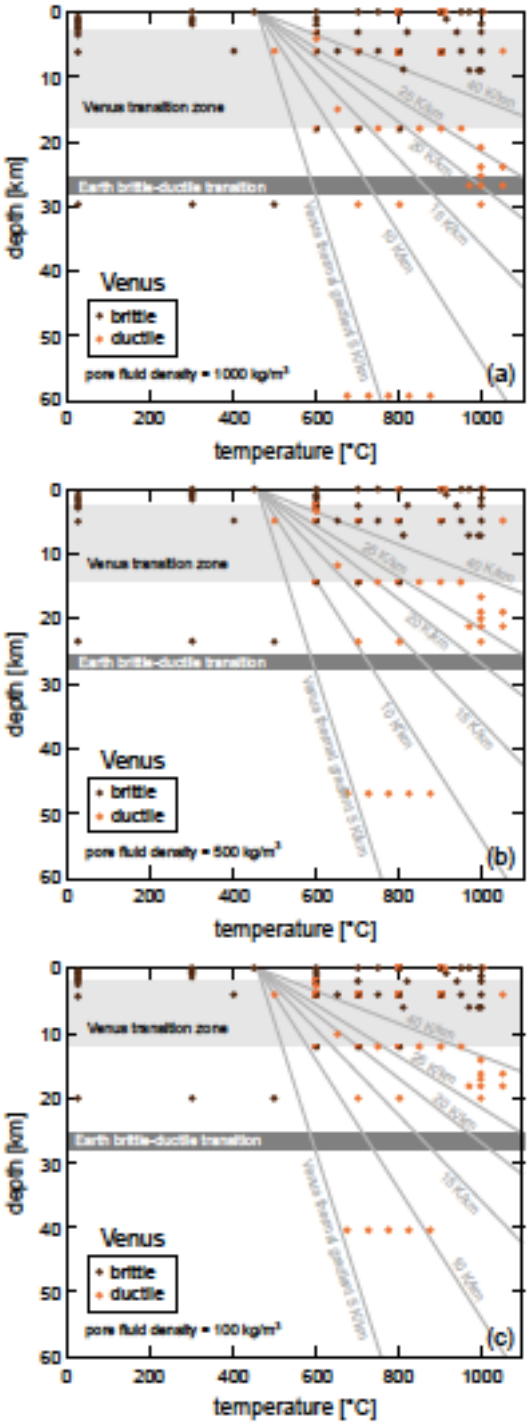

692

693 **Fig. 4**: Failure mode maps (brittle or ductile) for Venus assuming a surface gravity of 8.87 m/s^2 and
694 an average surface temperature of 460 °C. Due to the uncertainty in the pore pressure gradient we
695 provide three scenarios. (a) That the pore fluid has a constant density of 1000 kg/m^3 (i.e. the same
696 as Earth; yielding a pore pressure gradient of ~8.9 MPa/km). (b) That the pore fluid has a constant
697 density of 500 kg/m^3 (yielding a pore pressure gradient of ~4.4 MPa/km). (c) That the pore fluid has
698 a constant density of 100 kg/m^3 (yielding a pore pressure gradient of ~0.89 MPa/km). Due to the

699 uncertainty in the thermal gradient we provide a range from 5 to 40 °C/km. See text for details.

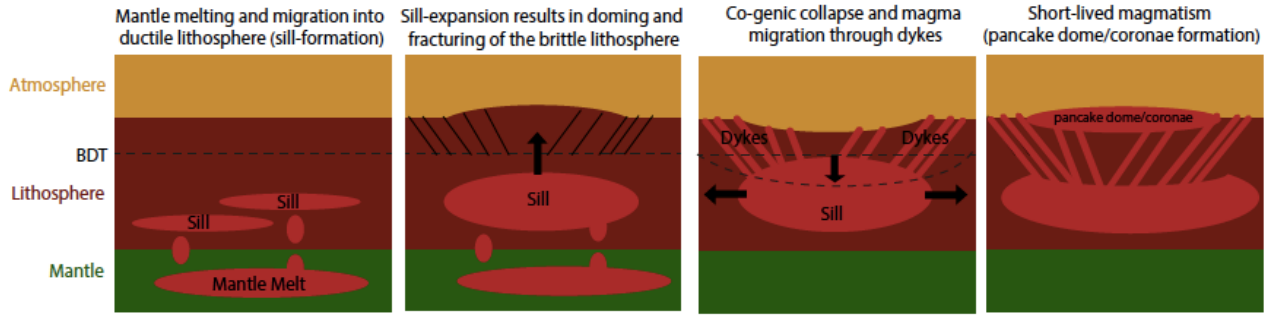

700

701 **Fig. 5**: The formation of coronae on Venus. This cartoon depicts sill emplacement and growth,
702 followed by uplift and faulting of the crust above the brittle-ductile transition (BDT). The schematic
703 also shows how this only leads to volcanism after the magma chamber makes physical contact with
704 faults (see text for more details; not to scale). Arrows indicate directions of main differential
705 stresses.

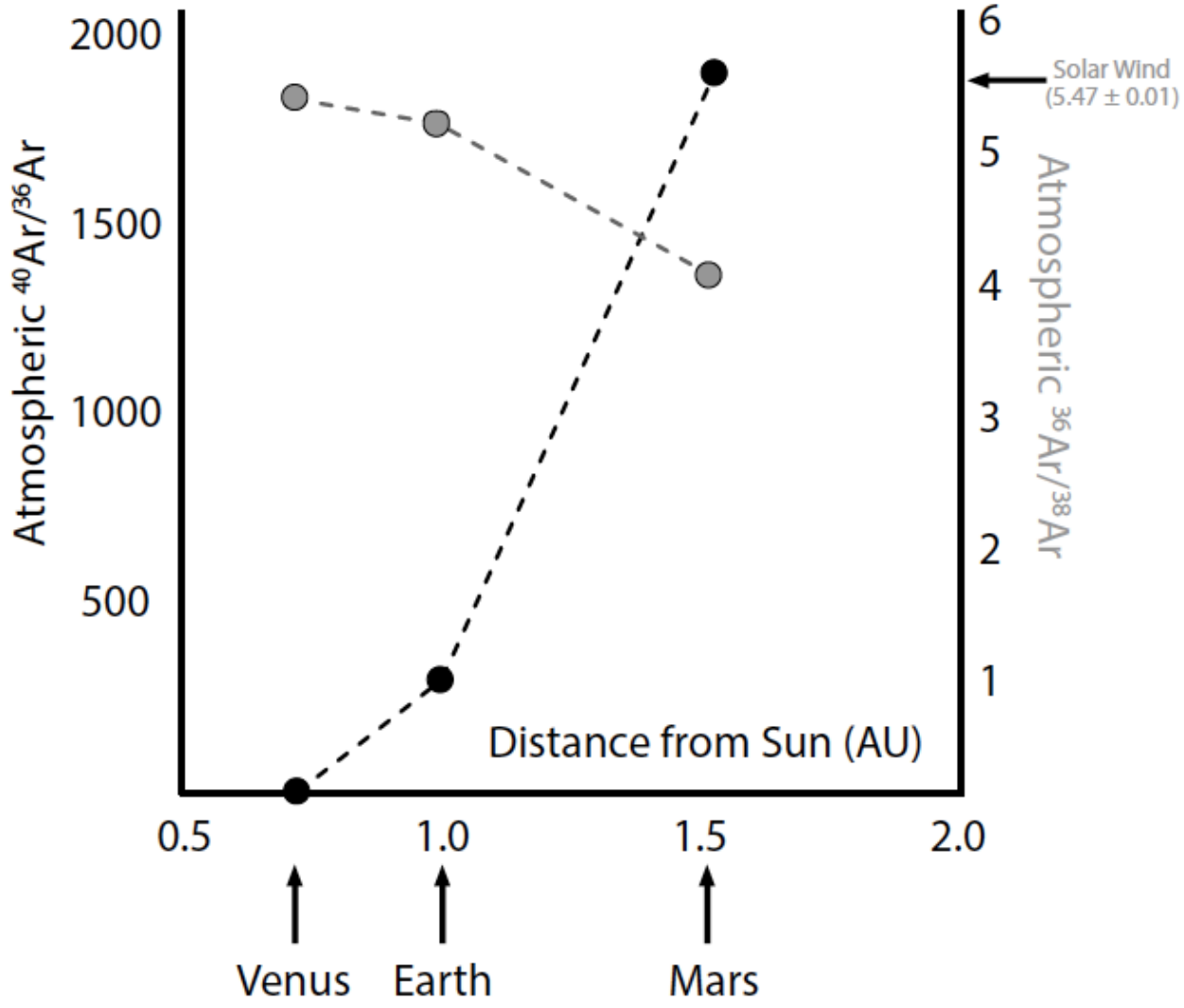

706

707 **Fig. 6**: The atmospheric argon isotope composition of Earth, Mars, and Venus (data from Istomin et

708 al., 1979; Hoffman et al., 1980b; Porcelli and Pepin, 2002; Mahaffy et al., 2013).

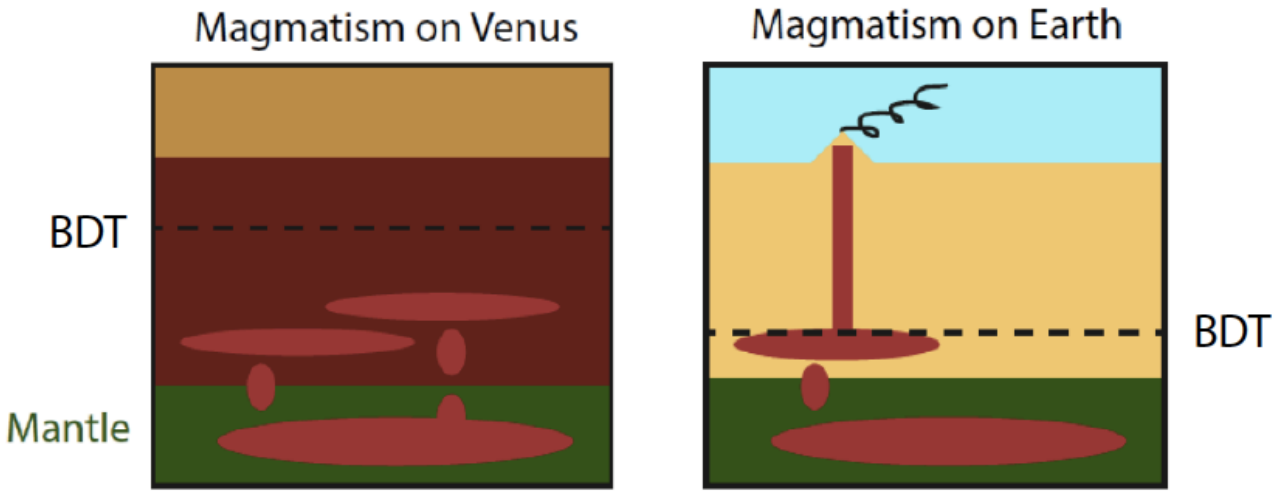

709

710 **Fig. 7**: Schematic illustration showing the relative differences for magma transport within the
711 lithosphere on Earth and Venus. The cartoon shows that primary magma chambers on Venus rely
712 on diapirism to move towards the surface, leading to stagnation and crystallisation (on average).
713 Conversely for Earth, primary magma chambers can force dyking in the overlying (brittle)
714 lithosphere and initiate volcanism.

715

716 **Table caption**

Reference	*Pc* (MPa)	*Pp* (MPa)	*Peff* (MPa)	*T* (°C)	σ_p (MPa)	Failure mode	Notes
Griggs et al. 1960	500	0	500	25	1668	Brittle	Basalt
Griggs et al. 1960	500	0	500	300	1390	Brittle	Basalt
Griggs et al. 1960	500	0	500	500	1080	Brittle	Basalt
Griggs et al. 1960	500	0	500	700	-	Ductile	Basalt
Griggs et al. 1960	500	0	500	800	-	Ductile	Basalt
Caristan 1982	0	0	0	950	199	Brittle	Maryland diabase; strain rate = 10^{-3} s^{-1}
Caristan 1982	0	0	0	970	223	Brittle	Maryland diabase; strain rate = 10^{-5} s^{-1}
Caristan 1982	0	0	0	995	193	Brittle	Maryland diabase; strain rate = 10^{-3} s^{-1}
Caristan 1982	30	0	30	1000	370	Brittle	Maryland diabase; strain rate = 10^{-3} s^{-1}
Caristan 1982	50	0	50	1000	440	Brittle	Maryland diabase; strain rate = 10^{-3} s^{-1}
Caristan 1982	150	0	150	810	780	Brittle	Maryland diabase; strain rate = 10^{-6} s^{-1}
Caristan 1982	150	0	150	970	385	Brittle	Maryland diabase; strain rate = 10^{-6} s^{-1}
Caristan 1982	150	0	150	994	535	Brittle	Maryland diabase; strain rate = 10^{-3} s^{-1}
Caristan 1982	150	0	150	1000	566	Brittle	Maryland diabase; strain rate = 10^{-4} s^{-1}
Caristan 1982	150	0	150	1000	561	Brittle	Maryland diabase; strain rate = 10^{-5} s^{-1}
Caristan 1982	150	0	150	1000	573	Brittle	Maryland diabase; strain rate = 10^{-5} s^{-1}
Caristan 1982	350	0	350	1000	-	Ductile	Maryland diabase; strain rate = 10^{-5} s^{-1}
Caristan 1982	400	0	400	1000	-	Ductile	Maryland diabase; strain rate = 10^{-4} s^{-1}
Caristan 1982	425	0	425	1000	-	Ductile	Maryland diabase; strain rate = 10^{-4} s^{-1}
Caristan 1982	425	0	425	1000	-	Ductile	Maryland diabase; strain rate = 10^{-5} s^{-1}
Caristan 1982	425	0	425	1000	-	Ductile	Maryland diabase; strain rate = 10^{-6} s^{-1}
Caristan 1982	450	0	450	1000	-	Ductile	Maryland diabase; strain rate = 10^{-5} s^{-1}
Shimada and Yukutake 1982	57	0	57	25	400	Brittle	Yakuno basalt; Porosity = 0.07; strain rate = 10^{-5} s^{-1}
Shimada and Yukutake 1982	107	0	107	25	415	Brittle	Yakuno basalt; Porosity = 0.07; strain rate = 10^{-5} s^{-1}
Bauer et al. 1981	50	0	50	25	540	Brittle	Cuerbio basalt; Porosity = 0.05-0.08; strain rate = 10^{-4} s^{-1}

Bauer et al. 1981	50	0	50	25	400	Brittle	Cuerbio basalt; Porosity = 0.05-0.08; strain rate = 10^{-4} s^{-1}
Bauer et al. 1981	50	0	50	600	300	Brittle	Cuerbio basalt; Porosity = 0.05-0.08; strain rate = 10^{-4} s^{-1}
Bauer et al. 1981	50	0	50	600	340	Brittle	Cuerbio basalt; Porosity = 0.05-0.08; strain rate = 10^{-4} s^{-1}
Bauer et al. 1981	50	0	50	700	300	Brittle	Cuerbio basalt; Porosity = 0.05-0.08; strain rate = 10^{-4} s^{-1}
Bauer et al. 1981	50	0	50	940	125	Brittle	Cuerbio basalt; Porosity = 0.05-0.08; strain rate = 10^{-4} s^{-1}
Bauer et al. 1981	50	0	50	940	200	Brittle	Cuerbio basalt; Porosity = 0.05-0.08; strain rate = 10^{-4} s^{-1}
Bauer et al. 1981	50	0	50	1000	100	Brittle	Cuerbio basalt; Porosity = 0.05-0.08; strain rate = 10^{-4} s^{-1}
Bauer et al. 1981	100	0	100	700	465	Brittle	Cuerbio basalt; Porosity = 0.05-0.08; strain rate = 10^{-4} s^{-1}
Bauer et al. 1981	100	0	100	900	240	Brittle	Cuerbio basalt; Porosity = 0.05-0.08; strain rate = 10^{-4} s^{-1}
Bauer et al. 1981	100	0	100	950	110	Brittle	Cuerbio basalt; Porosity = 0.05-0.08; strain rate = 10^{-4} s^{-1}
Bauer et al. 1981	100	0	100	1000	180	Brittle	Cuerbio basalt; Porosity = 0.05-0.08; strain rate = 10^{-4} s^{-1}
Bauer et al. 1981	100	50	50	820	180	Brittle	Cuerbio basalt; Porosity = 0.05-0.08; strain rate = 10^{-4} s^{-1}
Shimada 1986	57	0	57	25	410	Brittle	Yakuno basalt; Porosity = 0.07; strain rate = 10^{-5} s^{-1}
Duclos and Paquet 1991	0	0	0	300	399	Brittle	Alkaline basalt; partially glassy; strain rate = 10^{-6} s^{-1}
Duclos and Paquet 1991	0	0	0	600	430	Brittle	Alkaline basalt; partially glassy; strain rate = 10^{-6} s^{-1}
Duclos and Paquet 1991	0	0	0	700	445	Brittle	Alkaline basalt; partially glassy; strain rate = 10^{-6} s^{-1}
Duclos and Paquet 1991	0	0	0	750	430	Brittle	Alkaline basalt; partially glassy; strain rate = 10^{-6} s^{-1}
Duclos and Paquet 1991	0	0	0	800	-	Ductile	Alkaline basalt; partially glassy; strain rate = 10^{-6} s^{-1}
Duclos and Paquet 1991	0	0	0	900	-	Ductile	Alkaline basalt; partially glassy; strain rate = 10^{-6} s^{-1}
Duclos and Paquet 1991	0	0	0	1000	-	Ductile	Alkaline basalt; partially glassy; strain rate = 10^{-6} s^{-1}
Hacker and Christie 1991	1000	0	1000	675	-	Ductile	Tholeiitic basalt; partially glassy; 0.5 wt.% water added; strain rate = 10^{-4} – 10^{-7} s^{-1}
Hacker and Christie 1991	1000	0	1000	725	-	Ductile	Tholeiitic basalt; partially glassy; 0.5 wt.% water added; strain rate = 10^{-4} – 10^{-7} s^{-1}
Hacker and Christie 1991	1000	0	1000	775	-	Ductile	Tholeiitic basalt; partially glassy; 0.5 wt.% water added; strain rate = 10^{-4} – 10^{-7} s^{-1}
Hacker and Christie 1991	1000	0	1000	825	-	Ductile	Tholeiitic basalt; partially glassy; 0.5 wt.% water added; strain rate = 10^{-4} – 10^{-7} s^{-1}
Hacker and Christie 1991	1000	0	1000	875	-	Ductile	Tholeiitic basalt; partially glassy; 0.5 wt.% water added; strain rate = 10^{-4} – 10^{-7} s^{-1}
Schultz 1993	0	0	0	450	210	Brittle	Estimated strength value taken as 80% of the average uniaxial compressive strength for basalt; see Schultz (1993) for details
Mackwell et al. 1998	400	0	400	1000	-	Ductile	Dehydrated Maryland and Columbia diabase; creep test; strain rate = 10^{-5} – 10^{-7} s^{-1}
Mackwell et al. 1998	400	0	400	1050	-	Ductile	Dehydrated Maryland and Columbia diabase; creep test; strain rate = 10^{-5} – 10^{-7} s^{-1}
Mackwell et al. 1998	400	0	400	1050	-	Ductile	Dehydrated Maryland and Columbia diabase; creep test; strain rate = 10^{-5} – 10^{-7} s^{-1}
Mackwell et al. 1998	450	0	450	970	-	Ductile	Dehydrated Maryland and Columbia diabase; creep test; strain rate = 10^{-5} – 10^{-7} s^{-1}
Mackwell et al. 1998	450	0	450	1000	-	Ductile	Dehydrated Maryland and Columbia diabase; creep test; strain rate = 10^{-5} – 10^{-7} s^{-1}
Mackwell et al. 1998	450	0	450	1050	-	Ductile	Dehydrated Maryland and Columbia diabase; creep test; strain rate = 10^{-5} – 10^{-7} s^{-1}

Mackwell et al. 1998	500	0	500	1000	-	Ductile	Dehydrated Maryland and Columbia diabase; creep test; strain rate = 10^{-5} – 10^{-7} s^{-1}
Rocchi et al. 2004	0	0	0	300	89	Brittle	Vesuvius basalt; Porosity = 0.08-0.10; strain rate = 10^{-5} s^{-1}
Rocchi et al. 2004	0	0	0	300	104	Brittle	Etna “core” basalt; strain rate = 10^{-5} s^{-1}
Rocchi et al. 2004	0	0	0	300	35	Brittle	Etna “crust” basalt; strain rate = 10^{-5} s^{-1}
Rocchi et al. 2004	0	0	0	600	96	Brittle	Vesuvius basalt; Porosity = 0.08-0.10; strain rate = 10^{-5} s^{-1}
Rocchi et al. 2004	0	0	0	600	105	Brittle	Vesuvius basalt; Porosity = 0.08-0.10; strain rate = 10^{-5} s^{-1}
Rocchi et al. 2004	0	0	0	600	103	Brittle	Etna “core” basalt; strain rate = 10^{-5} s^{-1}
Rocchi et al. 2004	0	0	0	600	181	Brittle	Etna “core” basalt; strain rate = 10^{-5} s^{-1}
Rocchi et al. 2004	0	0	0	600	40.5	Brittle	Etna “crust” basalt; strain rate = 10^{-5} s^{-1}
Rocchi et al. 2004	0	0	0	700	33	Brittle	Etna “crust” basalt; strain rate = 10^{-5} s^{-1}
Rocchi et al. 2004	0	0	0	800	42	Brittle	Vesuvius basalt; Porosity = 0.08-0.10; strain rate = 10^{-5} s^{-1}
Rocchi et al. 2004	0	0	0	800	43	Brittle	Etna “core” basalt; strain rate = 10^{-4} s^{-1}
Rocchi et al. 2004	0	0	0	800	25	Brittle	Etna “core” basalt; strain rate = 10^{-5} s^{-1}
Rocchi et al. 2004	0	0	0	800	17	Brittle	Etna “core” basalt; strain rate = 10^{-6} s^{-1}
Rocchi et al. 2004	0	0	0	800	20	Brittle	Etna “crust” basalt; strain rate = 10^{-4} s^{-1}
Rocchi et al. 2004	0	0	0	900	50	Brittle	Vesuvius basalt; Porosity = 0.08-0.10; strain rate = 10^{-4} s^{-1}
Rocchi et al. 2004	0	0	0	900	38	Brittle	Vesuvius basalt; Porosity = 0.08-0.10; strain rate = 10^{-5} s^{-1}
Rocchi et al. 2004	0	0	0	900	29	Brittle	Vesuvius basalt; Porosity = 0.08-0.10; strain rate = 10^{-5} s^{-1}
Rocchi et al. 2004	0	0	0	900	31	Brittle	Vesuvius basalt; Porosity = 0.08-0.10; strain rate = 10^{-6} s^{-1}
Rocchi et al. 2004	5	0	5	25	108	Brittle	Vesuvius basalt; Porosity = 0.08-0.10; strain rate = 10^{-5} s^{-1}
Rocchi et al. 2004	10	0	10	25	104	Brittle	Vesuvius basalt; Porosity = 0.08-0.10; strain rate = 10^{-5} s^{-1}
Rocchi et al. 2004	10	0	10	300	101	Brittle	Vesuvius basalt; Porosity = 0.08-0.10; strain rate = 10^{-5} s^{-1}
Rocchi et al. 2004	10	0	10	300	88	Brittle	Vesuvius basalt; Porosity = 0.08-0.10; strain rate = 10^{-5} s^{-1}
Rocchi et al. 2004	10	0	10	600	116	Brittle	Vesuvius basalt; Porosity = 0.08-0.10; strain rate = 10^{-5} s^{-1}
Rocchi et al. 2004	10	0	10	916	62	Brittle	Vesuvius basalt; Porosity = 0.08-0.10; strain rate = 10^{-5} s^{-1}
Rocchi et al. 2004	12	0	12	25	93	Brittle	Vesuvius basalt; Porosity = 0.08-0.10; strain rate = 10^{-5} s^{-1}
Rocchi et al. 2004	15	0	15	25	101	Brittle	Vesuvius basalt; Porosity = 0.08-0.10; strain rate = 10^{-5} s^{-1}
Rocchi et al. 2004	17	0	17	25	100	Brittle	Vesuvius basalt; Porosity = 0.08-0.10; strain rate = 10^{-5} s^{-1}
Rocchi et al. 2004	20	0	20	25	109	Brittle	Vesuvius basalt; Porosity = 0.08-0.10; strain rate = 10^{-5} s^{-1}
Rocchi et al. 2004	20	0	20	300	95	Brittle	Vesuvius basalt; Porosity = 0.08-0.10; strain rate = 10^{-5} s^{-1}
Rocchi et al. 2004	20	0	20	300	91	Brittle	Vesuvius basalt; Porosity = 0.08-0.10; strain rate = 10^{-5} s^{-1}
Rocchi et al. 2004	20	0	20	600	118	Brittle	Vesuvius basalt; Porosity = 0.08-0.10; strain rate = 10^{-5} s^{-1}
Rocchi et al. 2004	30	0	30	25	112	Brittle	Vesuvius basalt; Porosity = 0.08-0.10; strain rate = 10^{-5} s^{-1}
Rocchi et al. 2004	30	0	30	25	103	Brittle	Vesuvius basalt; Porosity = 0.08-0.10; strain rate = 10^{-5} s^{-1}
Rocchi et al. 2004	30	0	30	300	105	Brittle	Vesuvius basalt; Porosity = 0.08-0.10; strain rate = 10^{-5} s^{-1}
Rocchi et al. 2004	30	0	30	300	87	Brittle	Vesuvius basalt; Porosity = 0.08-0.10; strain rate = 10^{-5} s^{-1}
Rocchi et al. 2004	30	0	30	600	104	Brittle	Vesuvius basalt; Porosity = 0.08-0.10; strain rate = 10^{-5} s^{-1}
Rocchi et al. 2004	30	0	30	604	79	Brittle	Vesuvius basalt; Porosity = 0.08-0.10; strain rate = 10^{-5} s^{-1}

Rocchi et al. 2004	0	0	0	900	-	Ductile	Etna "crust" basalt; strain rate = 10^{-5} s^{-1}
Rocchi et al. 2004	0	0	0	912	-	Ductile	Etna "core" basalt; strain rate = 10^{-5} s^{-1}
Rocchi et al. 2004	0	0	0	1001	-	Ductile	Vesuvius basalt; Porosity = 0.08-0.10; strain rate = 10^{-5} s^{-1}
Apuani et al. 2005	4	0	4	25	98	Brittle	Vigna Vecchia basalt (Stromboli)
Apuani et al. 2005	4	0	4	25	72	Brittle	Vigna Vecchia basalt (Stromboli)
Apuani et al. 2005	4	0	4	25	67	Brittle	Vigna Vecchia basalt (Stromboli)
Apuani et al. 2005	8	0	8	25	88	Brittle	Vigna Vecchia basalt (Stromboli)
Apuani et al. 2005	8	0	8	25	99	Brittle	Vigna Vecchia basalt (Stromboli)
Apuani et al. 2005	12	0	12	25	104	Brittle	Vigna Vecchia basalt (Stromboli)
Apuani et al. 2005	12	0	12	25	109	Brittle	Vigna Vecchia basalt (Stromboli)
Apuani et al. 2005	16	0	16	25	54	Brittle	Vigna Vecchia basalt (Stromboli)
Apuani et al. 2005	16	0	16	25	62	Brittle	Vigna Vecchia basalt (Stromboli)
Apuani et al. 2005	16	0	16	25	87	Brittle	Vigna Vecchia basalt (Stromboli)
Apuani et al. 2005	16	0	16	25	94	Brittle	Vigna Vecchia basalt (Stromboli)
Apuani et al. 2005	20	0	20	25	56	Brittle	Vigna Vecchia basalt (Stromboli)
Apuani et al. 2005	20	0	20	25	109	Brittle	Vigna Vecchia basalt (Stromboli)
Apuani et al. 2005	20	0	20	25	178	Brittle	Vigna Vecchia basalt (Stromboli)
Benson et al. 2007	60	20	40	25	475	Brittle	Etna basalt; porosity = 0.04; strain rate = 10^{-6} s^{-1}
Ougier-Simonin et al. 2010	15	0	15	25	370	Brittle	Seljadur basalt; porosity = 0.05; strain rate = 10^{-6} s^{-1}
Heap et al. 2011	30	20	10	25	291	Brittle	Etna basalt; porosity = 0.4; strain rate = 10^{-5} s^{-1}
Heap et al. 2011	50	20	30	25	287	Brittle	Etna basalt; porosity = 0.4; strain rate = 10^{-5} s^{-1}
Heap et al. 2011	70	20	50	25	504	Brittle	Etna basalt; porosity = 0.4; strain rate = 10^{-5} s^{-1}
Heap et al. 2011	50	20	30	25	375	Brittle	Etna basalt; porosity = 0.4; creep test; strain rate = 10^{-6} s^{-1}
Heap et al. 2011	50	20	30	25	357	Brittle	Etna basalt; porosity = 0.4; creep test; strain rate = 10^{-7} s^{-1}
Heap et al. 2011	50	20	30	25	329	Brittle	Etna basalt; porosity = 0.4; creep test; strain rate = 10^{-8} s^{-1}
Heap et al. 2011	50	20	30	25	304	Brittle	Etna basalt; porosity = 0.4; creep test; strain rate = 10^{-9} s^{-1}
Violay et al. 2012	100	0	100	400	1002	Brittle	Aphanitic basalt; porosity = 0.02; strain rate = 10^{-5} s^{-1}
Violay et al. 2012	100	0	100	400	902	Brittle	Porphyritic basalt; partially glassy; porosity = 0.02; strain rate = 10^{-5} s^{-1}
Violay et al. 2012	100	0	100	600	854	Brittle	Aphanitic basalt; porosity = 0.02; strain rate = 10^{-5} s^{-1}
Violay et al. 2012	100	0	100	700	508	Brittle	Aphanitic basalt; porosity = 0.02; strain rate = 10^{-5} s^{-1}
Violay et al. 2012	100	0	100	800	462	Brittle	Aphanitic basalt; porosity = 0.02; strain rate = 10^{-5} s^{-1}
Violay et al. 2012	100	0	100	800	446	Brittle	Aphanitic basalt; porosity = 0.02; strain rate = 10^{-5} s^{-1}
Violay et al. 2012	100	0	100	900	355	Brittle	Aphanitic basalt; porosity = 0.02; strain rate = 10^{-5} s^{-1}
Violay et al. 2012	300	0	300	600	749	Brittle	Aphanitic basalt; porosity = 0.02; strain rate = 10^{-5} s^{-1}
Violay et al. 2012	300	0	300	700	755	Brittle	Aphanitic basalt; porosity = 0.02; strain rate = 10^{-5} s^{-1}
Violay et al. 2012	300	0	300	800	518	Brittle	Aphanitic basalt; porosity = 0.02; strain rate = 10^{-5} s^{-1}
Violay et al. 2012	50	0	50	600	-	Ductile	Porphyritic basalt; partially glassy; porosity = 0.02; strain rate = 10^{-5} s^{-1}

Violay et al. 2012	70	0	70	600	-	Ductile	Porphyritic basalt; partially glassy; porosity = 0.02; strain rate = 10^{-5} s^{-1}
Violay et al. 2012	100	0	100	500	-	Ductile	Porphyritic basalt; partially glassy; porosity = 0.02; strain rate = 10^{-5} s^{-1}
Violay et al. 2012	100	0	100	600	-	Ductile	Porphyritic basalt; partially glassy; porosity = 0.02; strain rate = 10^{-5} s^{-1}
Violay et al. 2012	100	0	100	600	-	Ductile	Porphyritic basalt; partially glassy; porosity = 0.02; strain rate = 10^{-5} s^{-1}
Violay et al. 2012	100	0	100	700	-	Ductile	Porphyritic basalt; partially glassy; porosity = 0.02; strain rate = 10^{-5} s^{-1}
Violay et al. 2012	100	0	100	800	-	Ductile	Porphyritic basalt; partially glassy; porosity = 0.02; strain rate = 10^{-5} s^{-1}
Violay et al. 2012	100	0	100	800	-	Ductile	Porphyritic basalt; partially glassy; porosity = 0.02; strain rate = 10^{-5} s^{-1}
Violay et al. 2012	100	0	100	800	-	Ductile	Porphyritic basalt; partially glassy; porosity = 0.02; strain rate = 10^{-5} s^{-1}
Violay et al. 2012	100	0	100	900	-	Ductile	Porphyritic basalt; partially glassy; porosity = 0.02; strain rate = 10^{-5} s^{-1}
Violay et al. 2012	100	0	100	900	-	Ductile	Porphyritic basalt; partially glassy; porosity = 0.02; strain rate = 10^{-5} s^{-1}
Violay et al. 2012	100	0	100	900	-	Ductile	Porphyritic basalt; partially glassy; porosity = 0.02; strain rate = 10^{-5} s^{-1}
Violay et al. 2012	250	0	250	650	-	Ductile	Porphyritic basalt; partially glassy; porosity = 0.02; strain rate = 10^{-5} s^{-1}
Violay et al. 2012	300	0	300	600	-	Ductile	Porphyritic basalt; partially glassy; porosity = 0.02; strain rate = 10^{-5} s^{-1}
Violay et al. 2012	300	0	300	700	-	Ductile	Porphyritic basalt; partially glassy; porosity = 0.02; strain rate = 10^{-5} s^{-1}
Violay et al. 2012	300	0	300	750	-	Ductile	Porphyritic basalt; partially glassy; porosity = 0.02; strain rate = 10^{-5} s^{-1}
Violay et al. 2012	300	0	300	800	-	Ductile	Porphyritic basalt; partially glassy; porosity = 0.02; strain rate = 10^{-5} s^{-1}
Violay et al. 2012	300	0	300	800	-	Ductile	Aphanitic basalt; porosity = 0.02; strain rate = 10^{-5} s^{-1}
Violay et al. 2012	300	0	300	850	-	Ductile	Aphanitic basalt; porosity = 0.02; strain rate = 10^{-5} s^{-1}
Violay et al. 2012	300	0	300	900	-	Ductile	Aphanitic basalt; porosity = 0.02; strain rate = 10^{-5} s^{-1}
Violay et al. 2012	300	0	300	900	-	Ductile	Porphyritic basalt; partially glassy; porosity = 0.02; strain rate = 10^{-5} s^{-1}
Violay et al. 2012	300	0	300	950	-	Ductile	Aphanitic basalt; porosity = 0.02; strain rate = 10^{-5} s^{-1}
Adelinet et al. 2013	10	5	5	25	120	Brittle	Reykjanes basalt; porosity = 0.08; strain rate = 10^{-6} s^{-1}
Adelinet et al. 2013	80	76	4	25	118	Brittle	Reykjanes basalt; porosity = 0.08; strain rate = 10^{-6} s^{-1}
Violay et al. 2015	130	30	100	600	877	Brittle	Aphanitic basalt; porosity = 0.03; strain rate = 10^{-5} s^{-1}
Violay et al. 2015	130	30	100	650	834	Brittle	Aphanitic basalt; porosity = 0.03; strain rate = 10^{-5} s^{-1}
Violay et al. 2015	130	30	100	700	792	Brittle	Aphanitic basalt; porosity = 0.03; strain rate = 10^{-5} s^{-1}
Violay et al. 2015	130	30	100	750	699	Brittle	Aphanitic basalt; porosity = 0.03; strain rate = 10^{-5} s^{-1}
Violay et al. 2015	130	30	100	800	717	Brittle	Aphanitic basalt; porosity = 0.03; strain rate = 10^{-5} s^{-1}
Violay et al. 2015	130	30	100	900	382	Brittle	Aphanitic basalt; porosity = 0.03; strain rate = 10^{-5} s^{-1}
Violay et al. 2015	130	30	100	1050	-	Ductile	Aphanitic basalt; porosity = 0.03; strain rate = 10^{-5} s^{-1}

Schaefer et al. 2015	0	0	0	935	167	Brittle	Pacaya (Guatemala) basalt; porosity = 0.02; strain rate = 10^{-1} s^{-1}
Schaefer et al. 2015	0	0	0	935	162	Brittle	Pacaya (Guatemala) basalt; porosity = 0.05; strain rate = 10^{-1} s^{-1}
Schaefer et al. 2015	0	0	0	935	126	Brittle	Pacaya (Guatemala) basalt; porosity = 0.06; strain rate = 10^{-5} s^{-1}
Schaefer et al. 2015	0	0	0	935	59	Brittle	Pacaya (Guatemala) basalt; porosity = 0.19; strain rate = 10^{-1} s^{-1}
Schaefer et al. 2015	0	0	0	935	49	Brittle	Pacaya (Guatemala) basalt; porosity = 0.16; strain rate = 10^{-5} s^{-1}
Schaeffer et al. 2015	0	0	0	935	93	Brittle	Pacaya (Guatemala) basalt; porosity = 0.19; strain rate = 10^{-1} s^{-1}
Schaefer et al. 2015	0	0	0	935	44	Brittle	Pacaya (Guatemala) basalt; porosity = 0.19; strain rate = 10^{-5} s^{-1}
Schaefer et al. 2015	0	0	0	935	75	Brittle	Pacaya (Guatemala) basalt; porosity = 0.23; strain rate = 10^{-1} s^{-1}
Schaefer et al. 2015	0	0	0	935	64	Brittle	Pacaya (Guatemala) basalt; porosity = 0.21; strain rate = 10^{-5} s^{-1}
Schaefer et al. 2015	0	0	0	935	28	Brittle	Pacaya (Guatemala) basalt; porosity = 0.32; strain rate = 10^{-1} s^{-1}
Schaefer et al. 2015	0	0	0	935	16	Brittle	Pacaya (Guatemala) basalt; porosity = 0.31; strain rate = 10^{-5} s^{-1}
Zhu et al. 2016	20	10	10	25	281	Brittle	Etna basalt (EB_I); porosity = 0.05; strain rate = 10^{-5} s^{-1}
Zhu et al. 2016	20	10	10	25	240	Brittle	Etna basalt (EB_I); porosity = 0.05; strain rate = 10^{-5} s^{-1}
Zhu et al. 2016	20	10	10	25	221	Brittle	Etna basalt (EB_I); porosity = 0.05; strain rate = 10^{-5} s^{-1}
Zhu et al. 2016	20	10	10	25	327	Brittle	Etna basalt (EB_I); porosity = 0.05; strain rate = 10^{-5} s^{-1}
Zhu et al. 2016	30	10	20	25	329	Brittle	Etna basalt (EB_I); porosity = 0.05; strain rate = 10^{-5} s^{-1}
Zhu et al. 2016	30	10	20	25	361	Brittle	Etna basalt (EB_I); porosity = 0.05; strain rate = 10^{-5} s^{-1}
Zhu et al. 2016	40	10	30	25	399	Brittle	Etna basalt (EB_I); porosity = 0.05; strain rate = 10^{-5} s^{-1}
Zhu et al. 2016	50	10	40	25	403	Brittle	Etna basalt (EB_I); porosity = 0.05; strain rate = 10^{-5} s^{-1}
Zhu et al. 2016	60	10	50	25	500	Brittle	Etna basalt (EB_I); porosity = 0.05; strain rate = 10^{-5} s^{-1}
Zhu et al. 2016	60	10	50	25	493	Brittle	Etna basalt (EB_I); porosity = 0.05; strain rate = 10^{-5} s^{-1}
Zhu et al. 2016	60	10	50	25	561	Brittle	Etna basalt (EB_I); porosity = 0.05; strain rate = 10^{-5} s^{-1}
Zhu et al. 2016	80	10	70	25	563	Brittle	Etna basalt (EB_I); porosity = 0.05; strain rate = 10^{-5} s^{-1}
Zhu et al. 2016	90	10	80	25	560	Brittle	Etna basalt (EB_I); porosity = 0.05; strain rate = 10^{-5} s^{-1}
Zhu et al. 2016	90	10	80	25	574	Brittle	Etna basalt (EB_I); porosity = 0.05; strain rate = 10^{-5} s^{-1}
Zhu et al. 2016	90	10	80	25	655	Brittle	Etna basalt (EB_I); porosity = 0.05; strain rate = 10^{-5} s^{-1}
Zhu et al. 2016	110	10	100	25	658	Brittle	Etna basalt (EB_I); porosity = 0.04; strain rate = 10^{-5} s^{-1}
Zhu et al. 2016	160	10	150	25	753	Brittle	Etna basalt (EB_I); porosity = 0.05; strain rate = 10^{-5} s^{-1}
Zhu et al. 2016	60	10	50	25	365	Brittle	Etna basalt (EB_II); porosity = 0.08; strain rate = 10^{-5} s^{-1}
Zhu et al. 2016	90	10	80	25	349	Brittle	Etna basalt (EB_II); porosity = 0.08; strain rate = 10^{-5} s^{-1}
Zhu et al. 2016	20	10	10	25	224	Brittle	Etna basalt (EB_III); porosity = 0.05; strain rate = 10^{-5} s^{-1}
Zhu et al. 2016	60	10	50	25	434	Brittle	Etna basalt (EB_III); porosity = 0.05; strain rate = 10^{-5} s^{-1}
Zhu et al. 2016	90	10	80	25	543	Brittle	Etna basalt (EB_III); porosity = 0.05; strain rate = 10^{-5} s^{-1}

Zhu et al. 2016	110	10	100	25	640	Brittle	Etna basalt (EB_III); porosity = 0.05; strain rate = 10^{-5} s^{-1}
Zhu et al. 2016	160	10	150	25	798	Brittle	Etna basalt (EB_III); porosity = 0.05; strain rate = 10^{-5} s^{-1}

717

718 **Table 1**: Summary of the experimental conditions for the rock deformation experiments used in this
719 study (for the construction of Figs. 3, 4, and 5) (see also Heap et al., 2017). *Pc* = confining pressure;
720 *Pp* = pore fluid pressure; *Peff* = effective pressure; *T* = experimental temperature; σ_p = peak
721 differential stress (see Figure 1). In some cases, failure mode classification differs from that stated
722 in the original publication. Data not included in this compilation are uniaxial experiments
723 conducted at room temperature and instances of non-viscous ductile deformation (see text for
724 details).

725

References

Addington, E.A. 2001. A stratigraphic study of small volcano clusters on Venus. Icarus, 149, 16-36.

Adelinet, M., Fortin, J., Schubnel, A., and Guéguen, Y. 2013. Deformation modes in an Icelandic basalt: From brittle failure to localized deformation bands. *Journal of Volcanology and Geothermal Research*, *255*, 12-25.

Airey M.W., Mather T.A., Pyle D.M., Glaze L.S., Ghail R.C., Wilson C.F. 2015. Explosive volcanic activity on Venus: the roles of volatile contribution, degassing, and external environment. Planetary and Space Science, 113, 33–48.

Al-Harthi, A.A., Al-Amri, R.M., and Shehata, W.M. 1999. The porosity and engineering properties of vesicular basalt in Saudi Arabia. Engineering Geology, 54, 313-320.

Allègre, C.J., Hofmann, A., O'Nions, K. 1996. The Argon constraints on mantle structure. Geophyscial Research Letters, 23, 3555-3557.

Apuani, T., Corazzato, C., Cancelli, A., Tibaldi, A. 2005. Physical and mechanical properties of rock masses at Stromboli: a dataset for volcano instability evaluation. Bulletin of Engineering Geology and the Environment, 64, 419-431.

Basilevsky, A. T., Head, J. W. 2003. The surface of Venus. Reports on Progress in Physics, 66, 1699–1734.

Basilevsky, A. T., Head, J. W., Schaber, G. G., Strom, R. G. 1997. In Venus II (eds. S. W. Bougher, D. M. Hunten, and R. J. Phillips). University of Arizona Press, Tucson, pp. 1047-1087.

Baud, P., Klein, E., Wong, T.-F. 2004. Compaction localization in porous sandstones: Spatial evolution of damage and acoustic emission activity. Journal of Structural Geology 26 (4), 603-624.

Bauer, S.J., and Handin, J. 1983. Thermal expansion and cracking of three confined water-saturated igneous rocks to 800 °C. Rock Mechanics and Rock Engineering, 16, 181-198.

Becerril, L., Galindo, I., Gudmundsson, A., Morales, J. M. 2013. Depth of origin of magma in eruptions. Scientific Reports, 2762, doi:10.1038/srep02762.

Bell, D.R., Rossman, G.R. 1992. Water in the Earth's mantle: the role of nominally anhydrous minerals. Science, 255, 1391-1397.

Benson, P.M., Heap, M.J., Lavallée, Y., Flaws, A., Hess, K.-U., Selvadurai, A.P.S., and Dingwell, D.B. 2012. Laboratory simulations of tensile fracture development in a volcanic conduit via cyclic magma pressurisation. Earth and Planetary Science Letters, 349, 231-239.

Benson, P.M., Thompson, A.B., Meredith, P.G., Vinciguerra, S., and Young, R.P. 2007. Imaging slow failure in triaxially deformed Etna basalt using 3D acoustic-emission location and X-ray computed tomography. Geophysical Research Letters, 34, L03303, doi:10.1029/2006GL028721.

Bercovici, D., Ricard, Y. 2014. Plate tectonics, damage and inheritance. Nature, 508, 513-516.

757 Bolfan-Casanova, N., Keppler, H., Rubie, D.C. 2000. Water partitioning between nominally anhydrous minerals in the
758 $MgO–SiO_2–H_2O$ system up to 24 GPa: implications for the distribution of water in the Earth's mantle. Earth and
759 Planetary Science Letters, 182, 209–221.
760 Bougher, S. W., Hunten, D. M., and Phillips R. J., editors. 1997. Venus II, University of Arizona Press, Tucson.
761 Brace WF, Paulding BW, Scholz CH. 1966. Dilatancy in the fracture of crystalline rocks. Journal of Geophysical
762 Research, 71, 3939–3953.
763 Brantut, N., Heap, M.J., Meredith, P.G., Baud, P. 2013. Time-dependent cracking and brittle creep in crustal rocks: A
764 review. Journal of Structural Geology, 52, 17-43.
765 Brooker, R.A., Du, Z., Blundy, J.D., Kelley, S.P., Allan, N.L., Wood, B.J., Chamorro, M., Wartho, J-A., and Purton,
766 J.A. 2003. The 'zero charge' partitioning behaviour of noble gases during mantle melting. Nature, 423, 738-741.
767 Brown, C.D., Grimm, R.E. 1997. Tessera deformation and the contemporaneous thermal state of the plateau highlands,
768 Venus. Earth and Planetary Science Letters, 147, 1-10.
769 Brown, C.D., Grimm, R.E. 1999. Recent tectonic and lithospheric thermal evolution of Venus. Icarus, 139, 40-48.
770 Bullock, M.A., Grinspoon, D.H. 2001. The Recent Evolution of Climate on Venus, Icarus, 150, 19-37.
771 Burov, E., Gerya, T. 2014. Asymmetric three-dimensional topography over mantle plumes. Nature, 513, 85-89.
772 Burt JD, Head JW. 1992. Thermal buoyancy on Venus: underthrusting vs. subduction. Geophysical. Research Letters,
773 19, 1707–1710.
774 Byrne, P., van Wyk de Vries, B., Murray, J., Troll, V. 2009. The geometry of volcano flank terraces on Mars. Earth and
775 Planetary Science Letters, 281, 1–13.
776 Byrne, P.K., Holohan, E.P., Kervyn, M., van Wyk de Vries, B., Troll, V.R., Murray, J.B. 2013. A sagging-spreading
777 continuum of large volcano structure. Geology, 41, 339–342.
778 Campbell, B.A. P.G. Rogers. 1994. Bell Regio, Venus—integration of remote-sensing data and terrestrial analogs for
779 geologic analysis. Journal of Geophysical Research Letters: Planets, 99, 21153–21171.
780 Caristan, Y. 1982. The transition from high temperature creep to fracture in Maryland diabase, Journal of Geophysical
781 Research, 87, 6781-6790.
782 Carmichael, I.S., 2002. The andesite aqueduct: perspectives on the evolution of intermediate magmatism in west-central
783 (105e99_W) Mexico. Contributions to Mineralogy and Petrology, 143, 641-663.
784 Carr, M.H., Head, J.W. 2010. Geologic history of Mars. Earth and Planetary Science Letters, 294, 185-203.
785 Carr, M.H., Head, J.W. 2015. Martian surface/near-surface water inventory: Sources, sinks, and changes with time.
786 Geophysical Research Letters, 42, 726-732.
787 Cassata, W. S., Renne, P. R., Shuster, D. L. 2011. Argon diffusion in pyroxenes: Implications for thermochronometry
788 and mantle degassing. Earth and Planetary Science Letters, 304,407–416.

789 Chamorro Perez, EM; Brooker, RA; Wartho, JA; Wood, BJ; Kelley, SP; Blundy, JD. 2002. Ar and K partitioning
790 between clinopyroxene and silicate melt to 8 GPa. Geochimica Cosmochimica et Acta, 66, 507–519.
791 Cottrell, E. 2015. Global Distribution of Active Volcanoes. In Volcanic Hazards, Risks, and Disasters, Ed. Papale, P.
792 Elsevier, 1-14.
793 Crisp, J., 1984. Rates of magma emplacement and volcanic output. Journal of Volcanology and Geothermal Research,
794 20, 177-211.
795 Crumpler, L.S., Head, J.W., Campbell, D.B. 1986. Orogenic belts on Venus. Geology, 14, 1031-1034.
796 Dasgupta, R. 2013. Ingassing, storage, and outgassing of terrestrial carbon through geologic time. Reviews in
797 Mineralogy and Geochemistry, 75, 183–229.
798 Dingwell, D.B., Romano, C., Hess, K.U. 1996. The effect of water on the viscosity of haplogranitic melt under P-T-X
799 conditions relevant to silicic volcanism. Contributions to Mineralogy and Petrology, 124, 19-28.
800 Donahue, T.M. 1999. New analysis of hydrogen and deuterium escape from Venus. Icarus, 141, 226-235.
801 Donahue T.M. and Russell C.T. 1997. The Venus atmosphere and ionosphere and their interaction with the solar wind:
802 an overview. In Venus II (eds. S. W. Bougher, D. M. Hunten, and R. J. Phillips). University of Arizona Press,
803 Tucson, pp. 3–31.
804 Duclos, R., and Paquet, J. 1991. High-temperature behaviour of basalts—role of temperature and strain rate on
805 compressive strength and K_{IC} toughness of partially glassy basalts at atmospheric pressure. International Journal
806 of Rock Mechanics and Mining Sciences & Geomechanics Abstracts, 28, 71-76.
807 Ernst RE. 2007. Mafic–ultramafic large igneous provinces (LIPs): Importance of the pre-Mesozoic record. Episodes,
808 30, 108-114.
809 Esposito, L.W. 1984. Sulfur Dioxide: Episodic Injection Shows Evidence for Active Venus Volcanism. Science, 223,
810 1072-1074.
811 Evans B, Frederich JT, Wong T-F. 1990. The brittle-ductile transition in rocks: recent experimental and theoretical
812 progress. In Duba AG, Durham WB, Handin J, Wang HF (eds) The brittle-ductile transition in rocks. The Heard
813 volume. pp. 1-20, American Geophysical Union, Geophys Monograph 56, Washington.
814 Fagents, S.A., Wilson. L. 1995. Explosive volcanism on Venus: transient volcanic explosions as a mechanism for
815 localized pyroclast dispersal. Journal of Geophysical Research: Planets, 100, 26327–26338.
816 Farvert, J.R., R.A. Yund. 1992. Oxygen diffusion in a fine-grained quartz aggregate with wetted and non-wetted
817 microstructures. Journal of Geophysical Research, 97, 14017-14029.
818 Fegley, B., Prinn, R. G. 1989. Estimation of the rate of volcanism on Venus from reaction rate measurements. Nature,
819 337, 55-58.
820 Foley, B. J. 2015. The role of plate tectonic-climate coupling and exposed land area in the development of habitable

climates on rocky planets. The Astrophysical Journal, 812, 1-23.

Foley, B.J., Bercovici, D., Landuyt, W. 2012. The conditions for plate tectonics on super-Earths: inferences from convection models with damage, Earth and Planetary Science Letters, 331, 281–290.

Gaillard, F. Scaillet, B. 2014. A theoretical framework for volcanic degassing chemistry in a comparative planetology perspective and implications for planetary atmospheres. Earth and Planetary Science Letters, 403, 307–316.

Galgana, G.A., Grosfils, E.B., McGovern, P.J. 2013. Radial dike formation on Venus: Insights from models of uplift, flexure and magmatism. Icarus, 225, 538-547.

Ghail, R. 2015. Rheological and pertrological implications for a stagnant lid regime on Venus. Planetary and Space Science, 113, 2-9.

Ghail, R.C., Wilson, L. 2013. A pyroclastic flow deposit on Venus. Geological Society Special Publications, 401, London.

Ghent, R., Hansen, V.L. 1999. Structural and kinematic analysis of Eastern Ovda Regio, Venus: Implications for crustal plateau formation. Icarus, 139, 116-136.

Giordano, D., Russell, J.R., Dingwell, D.B. 2008. Viscosity of magmatic liquids: a model. Earth and Planetary Science Letters, 271, 123–134.

Glaze, L.S. Baloga, S.M. Wimert, J. 2011. Explosive volcanic eruptions from linear vents on Earth, Venus, and Mars: comparisons with circular vent eruptions. Journal of Geophysical Research: Planets, 12, 116-128.

Griffiths, R.W., Fink. J.H. 1992. The morphology of lava flows in planetary environments: predictions from analog experiments. Journal of Geophysical Research, 97, B13, 19739-19748.

Griggs, D.T., Turner, F.J., Heard, H.C. 1960. Deformation of rocks at 500 to 800°C, *in* Griggs, D.T., and Handin, J.W., eds., Rock Deformation, Geol. Soc. Amer., pp. 39–104 Mem. 79.

Grimm, R.E. 1994. Recent deformation rates on Venus. Journal of Geophysical Research: Planets, 99, 23163-23171.

Grimm, R.E., Solomon, S.C. 1988. Viscous relaxation of impact crater relief on Venus: Constraints on crustal thickness and thermal gradient. Journal of Geophysical Research: Solid Earth, 93, 11911-11929.

Grindrod, P.M., Stofan, E.R., Brian, A.W., Guest, J.E. 2006. The geological evolution of Atai Mons, Venus: a volcano-corona 'hybrid'. Journal of the Geological Society of London, 163, 265-275.

Grindrod, P.M., Hoogenboom, T. 2006. Venus: The corona conundrum. Astronomy & Geophysics, 47, 3-16.

Grindrod, P.M., Stofan, E.R., Guest, J.E. 2010. Volcanism and resurfacing on Venus at the full resolution of Magellan SAR data. Geophysical Research Letters, 37, doi: 10.1029/2010GL043424.

Grosfils, E.B., Head, J.W. 1994. The global distribution of giant radiating dike swarms on Venus: implications for the global stress state. Geophysical Research Letters, 21, 701-704.

Grosfils, E.B., S.M. Long, E.M. Venechuk, D.M. Hurwitz, J.W. Richards, B. Kastl, D.E. Drury, J. Hardin. 2011.

Geologic Map of the Ganiki Planitia Quadrangle (V-14), Venus [map] Scientific Investigations Map 3121, U.S. Geological Survey.

Gudmundsson, A. 2002. Emplacement and arrest of dykes and sheets in central volcanoes. Journal of Volcanology and Geothermal Research. 116, 279-298.

Gudmundsson, A. 2006. How local stresses control magma-chamber ruptures, dyke injections, and eruptions in composite volcanoes. Earth-Science Reviews, 79, 1-31.

Gudmundsson, A. 2011. Rock fractures in geological processes. Cambridge University Press. ISBN: 978-0-521-86392-6.

Hacker, B.R., Christie, J.M. 1991. Experimental deformation of a glassy basalt. Tectonophysics, *200*, 79-96.

Halliday, A. N. 2013. The origins of volatiles in the terrestrial planets. Geochimica et Cosmochimica Acta, 105, 146–171.

Hansen, V.L., Banks, B.K., Ghent, R.R. 1999. Tessera terrain and crustal plateaus on Venus. Geology, 27, 1071-1074.

Hansen, V.L., Willis, J.J. 1996. Structural analysis of a sampling of tesserae: Implications for Venus geodynamics, Icarus, 123, 296-312.

Hansen, V.L., Willis, J.J. 1998. Ribbon Terrain Formation, Southwestern Fortuna Tessera, Venus: Implications for Lithosphere Evolution. Icarus, 132, 321-343.

Harris, A.J.L., Rowland, S.K. 2009. Effusion rate controls on lava flow length and the role of heat loss: a review. In: Studies in Volcanology: The Legacy of George Walker (Eds: Thordarson, T., Self, S., Larsen, G., Rowland, S.K., Hoskuldsson, A.), Special Publications of IAVCEI, Geological Society of London, 2, 33-51.

Head, J.W., Crumpler, L.S., Aubele, J.C., Guest, J.E., Saunders, R.S. 1992. Venus volcanism: Classification of volcanic features and structures, associations, and global distribution from Magellan data. Journal of Geophysical Research, 97, 13153–13197.

Head, J.W., Solomon, S.C. 1981. Tectonic Evolution of the Terrestrial Planets. Science, 213, 62-76.

Head, J.W., Wilson, L. 1992. Magma reservoirs and neutral buoyancy zones on Venus: Implications for the formation and evolution of volcanic landforms. Journal of Geophysical Research, 97, 3877-3903.

Heap, M.J., Vinciguerra, S., Meredith, P.G. 2009. The evolution of elastic moduli with increasing damage during cyclic stressing of a basalt from Mt. Etna volcano. Tectonophysics, 471, 153-160.

Heap, M.J., Baud, P., Meredith, P.G., Vinciguerra, S., Bell, A.F., and Main, I.G. 2011. Brittle creep in basalt and its application to time-dependent volcano deformation. Earth and Planetary Science Letters, *307*, 71-82.

Heap, M. J., Farquharson, J.I., Baud, P., Lavallée, Y., Reuschlé, T. 2015. Fracture and compaction of andesite in a volcanic edifice. Bulletin of Volcanology, 77: 55 DOI: 10.1007/s00445-015-0938-7.

884 Heap, M.J., Byrne, P., Mikhail, S. 2017. Low surface gravitational acceleration of Mars results in a thick and weak
885 lithosphere: Implications for topography, volcanism, and hydrology. Icarus, 281, 103-114.
886 Herrick, R.R., Dufek, J., McGovern, P.J. 2005. Evolution of large shield volcanoes on Venus. Journal of Geophysical
887 Research, 110, DOI: 10.1029/2004JE002283.
888 Hess, K.U., Dingwell, D.B., Gennaro, C., and Mincione, V. 2001. Viscosity-tem- perature behavior of dry melts in the
889 Qz-Ab-Or system. Chemical Geology, 174, 133–142.
890 Hess, K.U., Dingwell, D.B. 1996. Viscosities of hydrous leucogranitic melts: A non-Arrhenian model. American
891 Mineralogist, 81, 1297–1300.
892 Hess, P.C., Head, J.W. 1990. Derivation of primary magmas and melting of crustal materials on Venus: Some
893 preliminary petrogenetic considerations. Earth, Moon, and Planets 50-51, 57-80.
894 Hill, G.J., Caldwell, T.G., Heise, W., Chertkoff, D.G., Bibby, H.M., Burgess, M.K., Cull, J.P., Cas. R.A.F. 2009.
895 Distribution of melt beneath Mount St Helens and Mount Adams inferred from magnetotelluric data. Nature
896 Geoscience, 211, 785-789.
897 Hirschmann, M.M. 2006. Water, melting, and the Earth deep H2O cycle. Annual Review of Earth and Planetary
898 Sciences, 34, 629-653.
899 Hoek, E., Bieniawski, Z.T. 1965. Brittle fracture propagation in rock under compression. International Journal of
900 Fracture, 1, 137–155.
901 Hoffman, J.H., Oyama, V.I., von Zahn, U. 1980a. Measurements of the Venus lower atmosphere composition: A
902 comparison of results. Journal of Geophysical Research, 85, 7871–7881.
903 Hoffman, J.H. Hodges Jr, R.R., Donahue, T.M., McElroy, M.B. 1980b. Composition of the Venus lower atmosphere
904 from the Pioneer Venus mass spectrometer. Journal of Geophysical Research, 85, 7882–7890.
905 Hunten, D. M. 1993. Atmospheric evolution of the terrestrial planets. Science, 259, 915– 920.
906 Istomin, V.G., Grechnev, K.V., Kochnev, V.A., 1980. Mass Spectrometer Measurements of the Composition of the
907 Lower Atmosphere of Venus. COSPAR Colloquia Series, Space Research — Proceedings of the Open Meetings
908 of the Working Groups on Physical Sciences of the Twenty-Second Plenary Meeting of COSPAR Bangalore,
909 India 29 May – 9 June 1979, 20, 215-218.
910 Ivanov, M.A., Head, J.W. 2013. The history of volcanism on Venus. Planetary and Space Science, 84, 66–92.
911 Jellinek, A.M., Lenardic, A., and Manga, M. 2002. The influence of interior mantle temperature on the structure of
912 plumes: Heads for Venus, tails for the Earth. Geophysical Research Letters, 29, 10.1029/2001GL014624.
913 Joesten, R., 1991. Grain-boundary diffusion kinetics in silicate and oxide minerals, in Diffusion, Atomic Ordering, and
914 Mass Transport, Advanced Physical Geochemistry, edited by J. Ganguly, vol. 8, pp. 345-395, Springer-Verlag,
915 New York.

916 Johnson, C.L., Richards, M.A. 2003. A conceptual model for the relationship between coronae and large-scale mantle
917 dynamics on Venus. Journal of Geophysical Research: Planets, 108 (E6), doi: 10.1029/2002JE001962.
918 Kaula, W. M. 1990. Venus: A contrast in evolution to Earth. Science, 247, 1191-1196.
919 Kaula W. M. 1991. Constraints on Venus evolution from radiogenic argon. Icarus, 139, 32-39.
920 Keddie, S.T., Head, J.W. 1995. Formation and evolution of volcanic edifices on the Dione-Regio rise, Venus. Journal of
921 Geophysical Research: Planets, 100, 11729–11754.
922 Kelley SP, Wartho J-A. 2000. Rapid kimberlite ascent and the significance of Ar-Ar ages in xenolith phlogopites.
923 Science, 289, 609-611.
924 Kelley, S. 2002. Excess argon in K-Ar and Ar-Ar geochronology. Chemical Geology, 188, 1–22.
925 Kelley. D.F., Barton, M. 2008. Pressures of Crystallization of Icelandic Magmas. Journal of Petrology, 49, 465-492.
926 Kohlstedt, D.L., Evans, B. Mackwell, S.J. 1995. Strength of the lithosphere: Constraints imposed by laboratory
927 experiments. Journal of Geophysical Research, 100, 17587-17602.
928 Kohlstedt, D.L. Keppler, H., Rubie, D.C. 1996. Solubility of water in the α, β and γ phases of $(Mg, Fe)_2SiO_4$.
929 Contributions to Mineralalogy and Petrology, 123, 345–357.
930 Krassilnikov, A.S., Kostama, V.-P., Aittola, M., Guseva, E.N., Cherkashina, O.S. 2012. Relation- ship of coronae,
931 regional plains and rift zones on Venus. Planetary and Space Science, 68, 56–75.
932 Krassilnikov, A.S., Head, J.W. 2003. Novae on Venus: Geology, classification, and evolution. Journal of Geophyscial
933 Research, 108, doi:10.1029/2002JE001983.
934 Kreslavsky, M.A., Ivanov, M.A., Head, J.W. 2015. The resurfacing history of Venus: constraints from buffered crater
935 densities. Icarus, 250, 438–450.
936 Leitner, J.J., Firneis, M.G. 2006. A review of Venusian surface heat flow estimates, AGU Chapman Conference on
937 Exploring Venus as a Terrestrial Planet.
938 Lécuyer, C., Simon, L., Guyot, F. 2010. Comparison of carbon, nitrogen and water budgets on Venus and the Earth.
939 Earth and Planetary Science Letters, 181, 33-40.
940 Mackwell, S.J., Zimmerman, M.E., Kohlstedt, D.L. 1998. High-temperature deformation of dry diabase with
941 application to tectonics on Venus. Journal of Geophysical Research, 103, 975-984.
942 Mahaffy, P.R., Webster, C.R., Atreya, S.K., Franz, H., Wong, M., Conrad, P.G., Harpold, D., Jones, J.J., Leshin, L.A.,
943 Manning, H., Owen, T., Pepin, R.O., Squyres, S., Trainer, M., MSL Science Team. 2013. Abundance and
944 Isotopic Composition of Gases in the Martian Atmosphere from the Curiosity Rover. Science, 341, 263-266.
945 Marcq, E., Belyaev, D., Montmessin, F., Fedorova, A., Bertaux, J-L., Vandaele, A.C., Neefs, E. 2011. An investigation
946 of the SO2 content of the venusian mesosphere using SPICAV-UV in nadir mode. Icarus, 211, 58–69.

947 Mather, T.A. 2008. Volcanism and the atmosphere: the potential role of the atmosphere in unlocking the reactivity of
948 volcanic emissions. Philosophical Transactions of the Royal Society A, 366, 4581–4595.
949 McCubbin, F. M. Hauri, E.H., Elardo, S.M., Vander Kaaden, K.E., Wang, J., Shearer Jr, C.K. 2012. Hydrous melting
950 of the martian mantle produced both depleted and enriched shergottites. Geology, 40, 683–686.
951 McGill, G.E. 2000. Geologic Map of the Sappho Patera Quadrangle (V-20), Venus [map] Geologic Investigations
952 Series I-2637, U.S. Geological Survey.
953 McGovern, P.J., Galgana, G.A., Verner, K.R., Herrick, R.R. 2014. New constraints on volcano-tectonic evolution of
954 large volcanic edifices on Venus from stereo topography-derived strain estimates. Geology, 42, 59-62.
955 McKenzie, D., Ford, P.G., Liu, F., Pettengill, G.H. 1992. Pancakelike domes on Venus. Journal of Geophysical
956 Research, 97, 15967–76.
957 McKinnon, W. B., Zahnle, K. J., Ivanov, B. A., Melosh, H. J. 1997. Cratering on Venus: Models and Observations. In
958 Venus II (eds. S. W. Bougher, D. M. Hunten, and R. J. Phillips). University of Arizona Press, Tucson, pp. 969–
959 1015.
960 Menéndez B, Zhu W, Wong T-f. 1996. Micromechanics of brittle faulting and cataclastic flow in Berea sandstone.
961 Journal of Structural Geology, 18, 1–16.
962 Michon, L., Ferrazzini, V., Di Muro, A., Villeneuve, N., Famin, V. 2015. Rift zones and magma plumbing system of
963 Piton de la Fournaise volcano: How do they differ from Hawaii and Etna? Journal of Volcanology and
964 Geothermal Research, 303, 112-129.
965 Mikhail, S., Sverjensky, D. A. 2014. Nitrogen speciation in upper mantle fluids and the origin of Earth's nitrogen-rich
966 atmosphere. Nature Geoscience, 7, 816–819.
967 Moore, J., Clague, D. 1992. Volcano growth and evolution of the island of Hawaii. Geological Socociety of America
968 Bullitin, 104, 1471-1484.
969 Morgan, W. J. 1971, Convection plumes in the lower mantle. Nature, 230, 42-43.
970 Mouginis-Mark, P.J. 2016. Geomorphology and volcanology of Maat Mons, Venus. Icarus 277, 433–441.
971 Namiki, N., Solomon. S. C. 1998. Volcanic degassing of argon and helium and the history of crustal production on
972 Venus. Journal of Geophysical Research, 103, 3655–3677.
973 Nimmo, F., McKenzie, D. 1998. Volcanism and tectonics on Venus. Annual Reviews of Earth and Planetary Sciences,
974 26, 23–51.
975 Nimmo, F., McKenzie, D. 1997. Convective thermal evolution of the upper mantles of Earth and Venus. Geophysical
976 Research Letters, 24, 1539–1542.
977 Nimmo, F., McKenzie, D. 1996, Modelling plume-related uplift, gravity and melting on Venus. Earth and Planetary
978 Science Letters, 145, 109–123.

O'Rourke, J., Korenaga, J. 2015. Thermal evolution of Venus with argon degassing. Icarus, 260, 128-140.

Ougier-Simonin, A., Fortin, J., Guéguen, Y., Schubnel, A., and Bouyer, F. 2011. Cracks in glass under triaxial conditions. International Journal of Engineering Science, 49, 105-121.

Paterson, M.S., Wong, T-F. 2005. Experimental Rock Deformation - The Brittle Field, Springer, New York, ISBN 978-3-540-26339-5.

Petford, N. 2003. Rheology of grantic magmas during ascent and emplacement. Annual Review of Earth and Planetary Sciences, 31, 399-427.

Pettengill, G.H., Ford, P.G., Johnson, W.T.K., Raney, R.K., Soderblom, L.A. 1991. Magellan: radar performance and data products. Science, 252, 260-265.

Phillips, R.J., Hanson, V.L. 1998. Geological evolution of Venus: Rises, plains, plumes, and plateau,. Science, 279, 1492-1497.

Plescia, J.B. 2004. Morphometric properties of Martian volcanoes. Journal of Geophysical Research, 109 (E3), doi: 10.1029/2002JE002031.

Pollack, J.B., Toon, O.B., Whitten, R.C., Boese, R., Ragent, B., Tomasko, M., Esposito, L,. Travis, L., Wiedman,D. 1980. Distribution and source of the UV absorption in Venus' atmosphere. Journal of Geophysical Research, 85, 8141-8150.

Porcelli, D., Pepin, R. O. 2003. The Origin of Noble Gases and Major Volatiles in the Terrestrial Planets, Treatise on Geochemistry, 319-347.

Roberts, K.M., Guest, J.E., Head, J.W., Lancaster, M.G. 1992. Mylitta Fluctus, Venus: Rift-related, centralized volcanism and the emplacement of large-volume flow units. Journal of Geophysical Research: Planets, 97, 15991-16015.

Robin, C.M.I., Jellinek, M., Thayalan, V., Lenardic, A. 2007. Transient mantle convection on Venus: the paradoxical coexistence of highlands and coronae in the BAT region. Earth and Planetary Science Letters, 256, 100–11

Rocchi, V., Sammonds, P.R., and Kilburn, C.R.J. 2004. Fracturing of Etnean and Vesuvian rocks at high temperatures and low pressures. Journal of Volcanology and Geothermal Research, 132, 137-157.

Rubin, A.M. 1995. Propagation of magma-filled cracks. Annual Review of Earth and Planetary Sciences, 23, 287-336.

Ruiz, J. 2007. The heat flow during the formation of ribbon terrains on Venus. Planetary and Space Science, 55, 2063-2070.

Rutter E. 1986. On the nomenclature of mode of failure transitions in rocks. Tectonophysics, 122, 381–387.

Schaefer, L.N., Kendrick, J.E., Oommen, T., Lavallée, Y., Chigna, G. 2015. Geomechanical rock properties of a basaltic volcano. Frontiers in Earth Sciences, doi: 10.3389/feart.2015.00029.

Scholz, C.H. 1968. Microfracturing and the inelastic deformation of rock in compression. Journal of Geophysical

1011 Research, 73, 1417–1432.
1012 Schubert, G., Bercovici, D., Glatzmaier, G.A. 2010. Mantle dynamics in Mars and Venus: Influence of an immobile
1013 lithosphere on three-dimensional mantle convection. Journal of Geophysical Research, 95, 14105-14129.
1014 Schultz, R.A. 1993. Brittle strength of basaltic rock masses with applications to Venus. Journal of Geophysical
1015 Research: Planets, 98, 10883-10895.
1016 Sclater JG, Jaupart C, Galson D. 1980. The heat flow through oceanic and continental crust and the heat loss of the
1017 Earth. Reviews in Geophysical Space Physics, 18, 269–311.
1018 Shalygin, E.V., Markiewicz, W.J., Basilevsky, A.T., Titov, D.V., Ignatiev, I.V., Head, J.W. 2015. Active volcanism on
1019 Venus in the Ganiki Chasma rift zone. Geophysical Research Letters, 42, 4762–4769.
1020 Shimada, M. 1986. Mechanism of deformation in a dry porous basalt at high pressures. Tectonophysics, 121, 153-173.
1021 Shimada, M., Ito, K., Cho, A. 1989. Ductile behavior of a fine-grained porous basalt at room temperature and pressures
1022 to 3 GPa. Physics of the Earth and Plantary Interiors, 55, 361-373.
1023 Shimada, M., Yukutake, H. 1982. Fracture and deformation of silicate rocks at high pressures in a cubic press.
1024 Advances in Earth and Planetary Sciences, 12, 193–205.
1025 Smith, D.K. 1996. Comparison of the shapes and sizes of seafloor volcanoes on Earth and “pancake” domes on Venus.
1026 Journal of Volcanology and Geothermal Research, 73, 47-64.
1027 Smith, R., Sammonds, P., Tuffen, H., Meredith, P.G. 2011. Evolution of the mechanics of the 2004–2008 Mt. St.
1028 Helens lava dome with time and temperature. Earth and Planetary Science Letters, 307, 191–200.
1029 Smrekar, S.E., Solomon, S.C. 1992. Gravitational spreading of high terrain in Ishtar Terra, Venus. Journal of
1030 Geophysical Research: Planets, 97, 16121-16148.
1031 Smrekar, S.E., Stofan, E.R. 1997. Corona formation and heat loss on Venus by coupled upwelling and delamination.
1032 Science, 277, 1289-1294.
1033 Smrekar, SE, Stofan, E.R., Mueller, N., Treiman, A., Elkins-Tanton, L., Helbert, J., Piccioni, G., Drossart, P. 2010.
1034 Recent hotspot volcanism on Venus from VIRTIS emissivity data. Science, 328, 605-608.
1035 Smyth, J.R., Frost, D.J., Nestola, F., Holl, C.M., Bromiley, G. 2006. Olivine hydration in the deep upper mantle: effects
1036 of temperature and silica activity. Geophysical Research Letters, 33, L15301.
1037 Solomatov, V.S., Moresi, S-N. 1996. Stagnant lid convection on Venus. Journal of Geophysical Research: Planets, 101,
1038 2156-2202.
1039 Solomon, S.C., Head, J. W. 1982. Mechanisms for lithospheric heat transport on Venus: Implications for tectonic style
1040 and volcanism. Journal of Geophysical Research: Solid Earth, 87, 9236-9246.
1041 Solomon, S.C., Head, J.W. 1984. Venus banded terrain: Tectonic models for band formation and their relationship to
1042 lithospheric thermal structur. Journal of Geophysical Research: Solid Earth, 89, 6885-6897.

1043 Squyres, S.W., Janes, D.M., Baer, G., Bindschadler, D.L., Schubert, G., Sharpton, V.L., Stofan, E.R. 1992. The
1044 morphology and evolution of coronae on Venus. Journal of Geophysical Research: Planets, 97, 13611-13634.
1045 Stofan, E.R., Sharpton, V.L., Schubert, G., Baer, G., Bindschadler, D.L., Janes, D.M., Squyres, S.W. 1992. Global
1046 distribution and characteristics of coronae and related features on Venus: Implications for origin and relation to
1047 mantle processes. Journal of Geophysical Research: Planets, 97, 13347-13378.
1048 Stofan, E.R., Smerkar, S.E;, Bindschadler, D.L., Senske, D.A. 1995. Large topographic rises on Venus: Implications for
1049 mantle upwelling. Journal of Geophysical Research: Planets, 100, 23317-23327.
1050 Stroncik, A., Klügel, A., Hansteen, T.H. 2009. The magmatic plumbing system beneath El Hierro (Canary Islands):
1051 constraints from phenocrysts and naturally quenched basaltic glasses in submarine rocks. Contributions to
1052 Mineralogy and Petrology, 157, 593–607.
1053 Taylor, S.R., McLennan, S (eds.). 2009. Planetary Crusts: Their Composition, Origin and Evolution. Cambridge
1054 University Press, 400pp.
1055 Thornhill. G.D. 1993. Theoretical modeling of eruption plumes on Venus. Journal of Geophysical Research: Planets,
1056 98, 9107–9111.
1057 Treiman A.H. 2007. Geochemistry of Venus' surface: Current limitations as future opportunities. Chapter in Exploring
1058 Venus as a Terrestrial Planet, AGU Monograph Series 176, 7-22.
1059 Turcotte, D.L., Schubert, G. 1988. Tectonic implications of radiogenic noble gases in planetary atmospheres. Icarus, 74,
1060 36-46.
1061 Turcotte, D.L. 1993. An episodic hypothesis for Venusian tectonics. Journal of Geophyscial Research: Planets, 98,
1062 2156-2202.
1063 Turcotte, D.L. 1995. How does Venus lose heat? Jounral of Geophyscial Research: Planets, 100, 16931-16940.
1064 Turcotte, D.L., Morein, G., Roberts, D., Malamud, B.D. 1999. Catastrophic resurfacing and episodic subduction on
1065 venus. Icarus, 139, 49–54.
1066 Turcotte, D.L., Willemann, R.J., Haxby, W.F., Norberry, J. 1981. Role of membrane stresses in the support of planetary
1067 topography. Journal of Geophysical Research, 86, 3951-3959.
1068 Violay, M., Gibert, B., Mainprice, D., Burg, J.-P. 2015. Brittle versus ductile deformation as the main control of the
1069 deep fluid circulation in oceanic crust. Geophysical Research Letters, DOI: 10.1002/2015GL063437.
1070 Violay, M., Gibert, B., Mainprice, D., Evans, B., Dautria, J.-M., Azias, P., and Pezard, P. 2012. An experimental study
1071 of the brittle-ductile transition of basalt at oceanic crust pressure and temperature conditions, Journal of
1072 Geophysical Research, DOI: 10.1029/2011JB008884.
1073 Watts, 2001. Isostasy and Flexure of the Lithosphere. Cambridge University Press. ISBN 0 521 62272 7.

1074 Wessel, P. 2001. Global distribution of seamounts inferred from gridded Geosat/ERS-1 altimetry. Journal of
1075 Geophysical Research, 106, 19431-19441.
1076 Williams, C.A., Connors, C., Dahlen, F.A., Price, E.J., Suppe, J. 1994. Effect of the brittle-ductile transition on the
1077 topography of compressive mountain belts on Earth and Venus. Journal of Geophysical Research: Solid Earth,
1078 99, 19947-19974.
1079 Wilson, L. 2009. Volcanism in the solar system. Nature Geoscience, 2, 389-397.
1080 Wilson, L., Head, J.W. 1983. A comparison of volcanic eruption processes on Earth, Moon, Mars, Io, and Venus.
1081 Nature, 302, 663-669.
1082 Wilson, L., Head, J.W. 1994. Mars: Review and analysis of volcanic eruption theory and relationships to observed
1083 landforms. Reviews of Geophysics, 32, 221-263.
1084 Wong, T-f, David, C, Zhu, W. 1997. The transition from brittle faulting to cataclastic flow in porous sandstones:
1085 mechanical deformation. Journal of Geophysical Research, 102, 3009–3025.
1086 Zhu, W., Baud, P., Vinciguerra, S., Wong, T-f. 2016. Micromechanics of brittle faulting and cataclastic flow in Mt.
1087 Etna basalt: Micromechanics of deformation in basalt. Journal of Geophysical Research, DOI:
1088 10.1002/2016JB012826.